

Detecting the resilience of soil moisture dynamics to drought periods as a function of soil type and climatic region

Nedal Aqel¹, Jannis Groh^{2,3}, Lutz Weihermüller², Ralf Gründling⁴, Andrea Carminati¹, Peter Lehmann¹

¹Physics of Soils and Terrestrial Ecosystems, ETH Zurich, Zurich, Switzerland

²Institute of Bio- and Geoscience IBG-3: Agrosphere, Forschungszentrum Jülich GmbH, Jülich, Germany

³Biogeochemistry and Gas Fluxes, Leibniz Institute for Agricultural and Landscape Research (ZALF), Müncheberg, Germany

⁴Department of Soil System Science, Helmholtz-Zentrum für Umweltforschung GmbH – UFZ, Halle, Germany

*Corresponding author, nedal.aqel@usys.ethz.ch, Universitätstrasse 16, 8092 Zurich, Switzerland

Abstract

Abrupt changes in climatic conditions and land management can cause permanent shifts in the soil hydraulic response to climatic inputs, impacting soil functions and established soil–climate interactions. To quantify the resilience of soil water content dynamics after abrupt changes in environmental conditions, we present a modelling framework that combines a neural network with seasonal trend analysis (STL). Using data from a series of lysimeters within the TERrestrial ENvironmental Observatories (TERENO)-SOILCan lysimeter network, we identified changes in the response of soil water content after an extremely hot and dry summer in Germany in 2018. The model incorporates meteorological variables decomposed into seasonal and long-term components, together with a categorical indicator of current moisture conditions. It was trained on data from a reference site with a stable soil water content response and applied to lysimeters from multiple origins exposed to contrasting climates. By analysing annual residual patterns—particularly mean bias over time—the soil water content dynamics are classified as being in a ‘stable’, ‘resilient’, or ‘changed’ state, reflecting whether the system maintains, recovers, or diverges from its original state. We found that soils preserved their response function to environmental forcing under typical conditions but exhibited changes in hydraulic behaviour when relocated to new environments, even when soil texture remained constant. The proposed method offers a scalable and non-invasive tool for tracking changes in soil water content response to climate change and provides early indicators of changes in essential soil functions and soil health status.

30 1. Introduction

31 Soil water content plays a fundamental role in hydrological processes and land–atmosphere interactions,
32 governing the exchange of water and energy at the Earth’s surface (Seneviratne et al., 2010; Sun et al.,
33 2025). It regulates key hydrological functions, including infiltration, runoff generation,
34 evapotranspiration, and groundwater recharge. Through these processes, soil water content influences
35 water availability, ecosystem productivity, and climatic conditions across local and global scales
36 (Bogena et al., 2015; Faticchi et al., 2020). Soil water content status and related soil environmental
37 conditions change with short- and long-term atmospheric processes. This response of soil water content
38 to atmospheric conditions, which is defined here as the ‘soil water content response function’,
39 determines, for example, whether anaerobic conditions are inhibited after heavy rainfall (through fast
40 percolation to deeper soil layers) and whether enough water remains available after dry periods for plant
41 growth, temperature regulation, and chemical reactions. In short, the soil water content response
42 function is an indicator of near-surface hydraulic functioning and land–atmosphere exchange processes,
43 which are relevant for several soil health–related aspects such as infiltration efficiency, surface aeration,
44 and runoff generation. This response function is shaped by soil formation processes and reflects
45 adaptation to the dominant climatic conditions (Kuzyakov and Zamanian, 2019; Sainju et al., 2022).
46 Accordingly, a change in the response function following extreme climatic events is likely to indicate
47 a change in soil health.

48 At the core of this study is the question of how changes in the soil water content response function, and
49 thus in soil properties and health, can be detected. The standard approach to determine the response
50 function is to apply physically based models, for example, by inverse modelling of soil water content
51 dynamics under varying boundary conditions (Šimůnek et al., 2016). These models require detailed
52 knowledge of soil hydraulic properties and extensive calibration, limiting their generalisation beyond
53 the spatial scale and the local conditions used for calibration (Lehmann et al., 2020; O. & Orth, 2021).
54 Additionally, soil hydraulic parameters for physically based models are usually obtained through soil
55 sampling or sensor installation, both of which disturb the soil structure, limiting the feasibility of
56 repeated measurements for long-term time-series analysis. Moreover, these models typically assume

57 static soil characteristics, failing to adequately represent structural changes in soil properties—such as
58 compaction, degradation, or organic matter loss—that can substantially alter hydraulic behaviour over
59 time (Fatichi et al., 2020; Melsen & Guse, 2021; Wankmüller et al., 2024). Most models also neglect
60 or oversimplify the hysteretic nature of the soil water retention curve, as well as seasonal changes in
61 soil hydraulic properties that can substantially alter infiltration, drainage, and plant water availability
62 (Aqel et al., 2024; Hannes et al., 2016; Herbrich & Gerke, 2017). Therefore, we used a non-invasive
63 approach based on neural networks as discussed below.

64 In recent years, artificial intelligence (AI), particularly neural networks, has emerged as a promising
65 alternative for modelling complex hydrological processes (Reichstein et al., 2019). These data-driven
66 models have demonstrated the ability to learn nonlinear relationships directly from observational
67 datasets without strong reliance on explicit physical equations (Kratzert et al., 2019; Mosavi et al., 2018;
68 Shen et al., 2018). Within soil hydrology, neural networks have been used to characterise hysteretic
69 soil–water behaviour from training data, improving the representation of wetting–drying cycles without
70 explicit hysteresis parameterisation (Aqel et al., 2024). They have also been applied to soil-moisture
71 time-series modelling using Long Short-Term Memory (LSTM) networks with recurrent architectures
72 suited to capture long-range temporal dependencies (Liu et al., 2023; O. & Orth, 2021). Across diverse
73 hydro-climatic regimes, LSTMs have been shown to effectively learn nonlinear relationships between
74 climatic inputs and soil water content, often matching or surpassing traditional physically based
75 approaches and demonstrating strong generalisation (Kratzert et al., 2019; J. Liu et al., 2022, 2023; O.
76 & Orth, 2021).

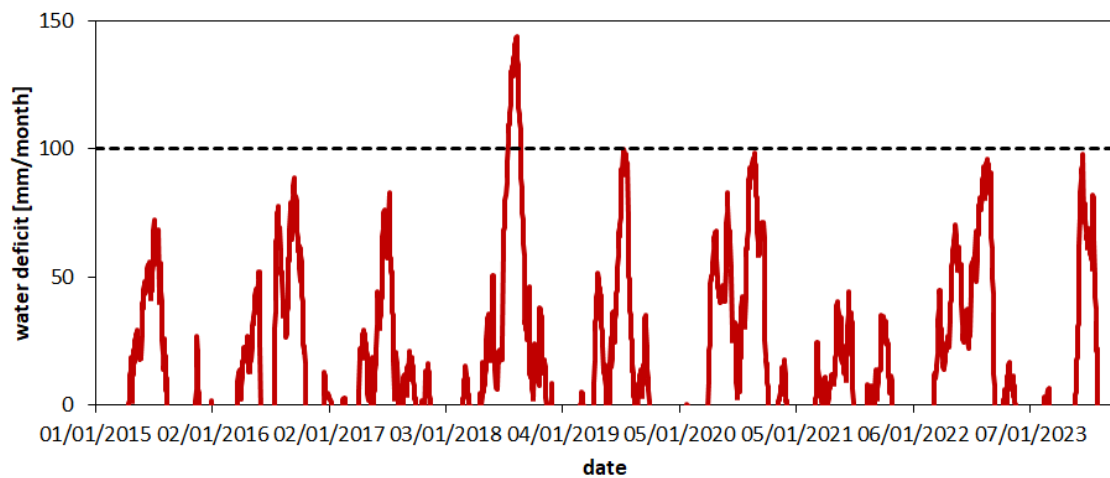
77 Independent of the chosen modelling approach, these models often ignore the fact that the soil water
78 content response function (i.e., the variations in soil water content following changes in atmospheric
79 conditions) can change over longer time scales. Experimental studies have shown that extreme events
80 such as drought can induce persistent shifts in soil water content dynamics, potentially leading to
81 alternative stable states (see Robinson et al., 2016; Quintana et al., 2023 and the section on illustrative
82 examples in Robinson et al., 2019). Moreover, changes in land use—such as forest conversion to
83 agriculture or bare land—alter soil hydraulic properties, with effects on infiltration, water retention, and

84 saturated hydraulic conductivity (Fu et al., 2021; Robinson et al., 2022). Considering that soil texture
85 (particle-size distribution) is assumed to remain constant at time scales of decades, the changes in the
86 response function are likely related to changes in soil structure and associated hydraulic properties
87 driven by structural reorganisation, wettability effects, root activity, or land-use changes rather than to
88 textural change.

89 Soil systems are subject to temporal change, yet models are often trained on historical datasets without
90 evaluating whether the system dynamics remain stable throughout the training period (Montanari et al.,
91 2013; Vaze et al., 2010). As a result, models may be applied to prediction settings where underlying
92 soil–climate interactions differ from those on which the model was trained. For example, a recent study
93 comparing different crop models using the TERENO-SOILCan set-up showed that predicting
94 agronomic and environmental variables under different climatic conditions from those represented in
95 the training datasets resulted in significant discrepancies between simulations and observations (Groh
96 et al., 2022). This underscores the critical need to assess whether site-specific representations of soil–
97 water behaviour remain valid over time (Hrachowitz et al., 2013) and highlights the need for more
98 adaptable modelling approaches under evolving environmental conditions (Blöschl et al., 2019; Milly
99 et al., 2008). A recent modelling framework by Jarvis et al. (2024) takes a major conceptual step forward
100 by explicitly representing soil-structure dynamics and their feedback on hydraulic behaviour. However,
101 as the authors emphasize, such process-based models still depend on detailed observational data to
102 constrain temporal changes in structure and hydraulic properties.

103 To address this gap, the present study introduces a framework based on neural networks and seasonal
104 trend decomposition. This framework is applied to quantify changes in the soil response function
105 following the 2018 summer drought, a Europe-wide extreme event. During this period, total
106 precipitation in central Europe fell to the lowest percentiles relative to the 1976–2005 reference
107 distribution. In Germany, the summer of 2018 was among the warmest on record and had the lowest
108 precipitation since 1881 (Xoplaki et al., 2025). The response of soil water content to this drought will
109 be analysed with a set of lysimeters. As shown in Fig. 1 for one of the study sites, the monthly water

110 deficit (potential evapotranspiration minus precipitation) peaked in summer 2018, indicating a strong
111 drought during this period.



112 **Figure 1** Variations in climatic conditions at Selhausen (SE) are expressed as the difference between potential
113 evapotranspiration (PET) and precipitation (P) accumulated over the preceding 30 days (one month). The
114 extreme summer of 2018 is manifested by a maximum monthly deficit of ~150 mm. Details on the calculation of
115 PET are provided in section 2.1.1.
116

117 Accordingly, the general objective of this study is to introduce a model framework to quantitatively
118 detect changes in the soil water content response function and classify it as ‘stable’, ‘resilient’, or
119 ‘changed’. These terms are used here as operational classes describing the temporal behaviour of the
120 response function, rather than as formal system-level properties or metrics as defined in ecological and
121 complex systems theory. In that framework, resilience is commonly understood as a system property
122 reflecting the capacity to absorb disturbance and recover, including both resistance to perturbation and
123 recovery towards pre-established levels. Stability, in contrast, refers to the tendency of system dynamics
124 to remain close to a reference state or equilibrium (Holling, 1973). In this study, ‘stable’ denotes that a
125 single response function remains valid throughout the entire monitoring period. ‘Resilient’ denotes a
126 temporary deviation from this response function following an extreme event (summer 2018), followed
127 by a return to the pre-event response within the observation window. In the third case, denoted here as
128 ‘changed’, the response function at the end of the observation period remains distinct from the pre-2018
129 reference response. Whether such a change represents a persistent transition to an alternative response
130 regime or a transient deviation with delayed recovery cannot be determined based on the available time
131 series.

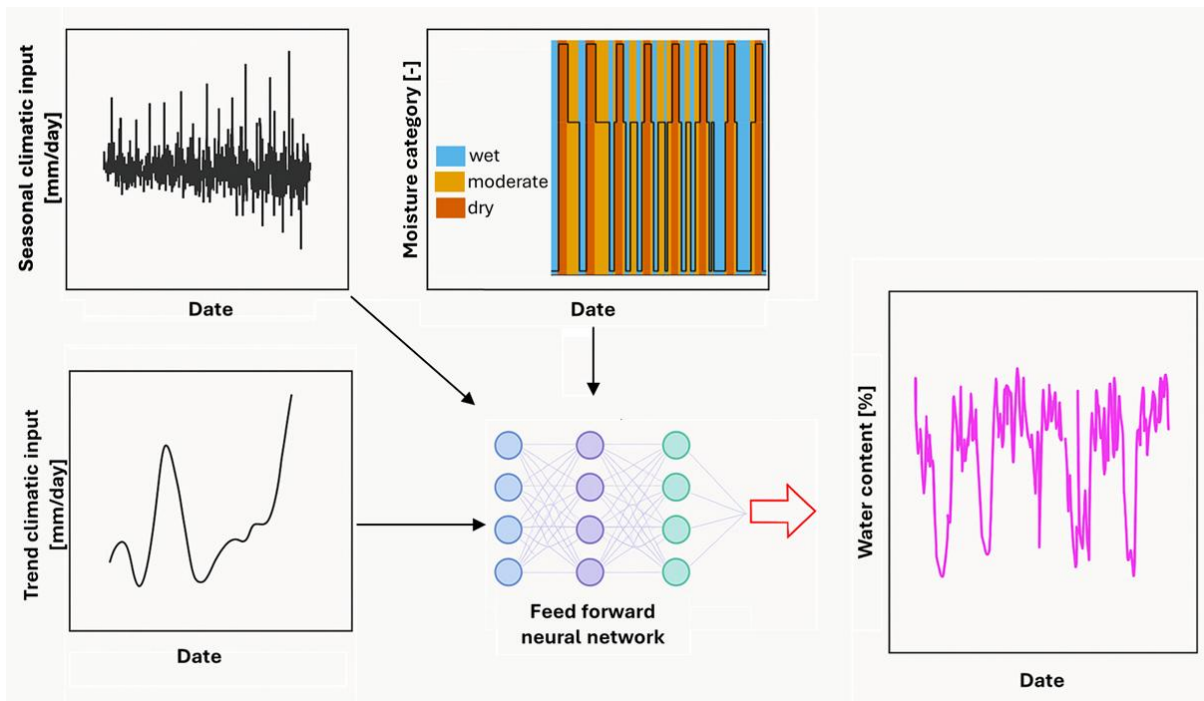
132

133

134 In principle, it would be possible to develop a quantitative framework to detect changes in the response
135 function exclusively based on experimental time-series data (without modelling), for example, by the
136 application of wavelet analysis (Ehrhardt et al., 2025). In this study, we adopt a predictive modelling
137 approach in which deviations between observed and simulated soil water content over time are used to
138 identify changes in the soil–climate response function. While the model also produces predictions of
139 soil water content, prediction accuracy is not the primary objective; instead, model–data deviations are
140 used to detect temporal drift in soil water response behaviour. The overall level of dynamic agreement
141 is summarized using the Nash–Sutcliffe efficiency, while the detection and classification of changes
142 rely on the temporal evolution of mean bias, as described in Section 2.5.

143 2. Materials and Methods

144 We developed a data-driven modelling framework that combines time-series decomposition of climatic
145 inputs with a feed-forward neural network to predict the daily soil water content (Fig. 2).



146

147 **Figure 2** Schematic overview of the modelling framework for daily soil water content prediction. Input features
148 include the analysis of a climatic variable (top left), its long-term trend component (bottom left), and the

149 *categorical soil water content state ('wet', 'moderate', 'dry'; top middle). These features, derived from observed*
150 *data, are used to train a feed-forward neural network (centre), which outputs daily predictions of volumetric*
151 *water content (right). The model thus captures temporal soil water content dynamics based on structured climate*
152 *signals and categorical conditions.*

153 The approach explicitly incorporates precipitation (P), potential evapotranspiration (PET), and their
154 difference (climatic water balance) as primary inputs. Each of these climate drivers was decomposed
155 into seasonal variations and long-term trend components using Seasonal-Trend decomposition (STL)
156 and was included as a separate feature in the model (Boergens et al., 2024; Cleveland et al., 1990). The
157 daily climatic water balance (WB) was included to reflect the net difference between P and PET, serving
158 as a proxy for wetting or drying conditions. Positive values indicate potential moisture accumulation
159 (e.g., during rainfall-dominated periods), while negative values reflect high evaporative demand and
160 drying conditions (e.g., during hot, dry spells). Including WB helps the model distinguish between
161 humid periods and dry ones. By providing WB alongside P and PET, the model can learn both the
162 individual and combined effects of precipitation and evaporative demand on soil water content
163 dynamics (Brocca et al., 2010; Uber et al., 2018). For example, it can infer that 10 mm of P during a
164 high-PET summer day (low positive or negative WB) is less likely to increase soil water content than
165 the same P on a cool, low-PET day (high positive WB).

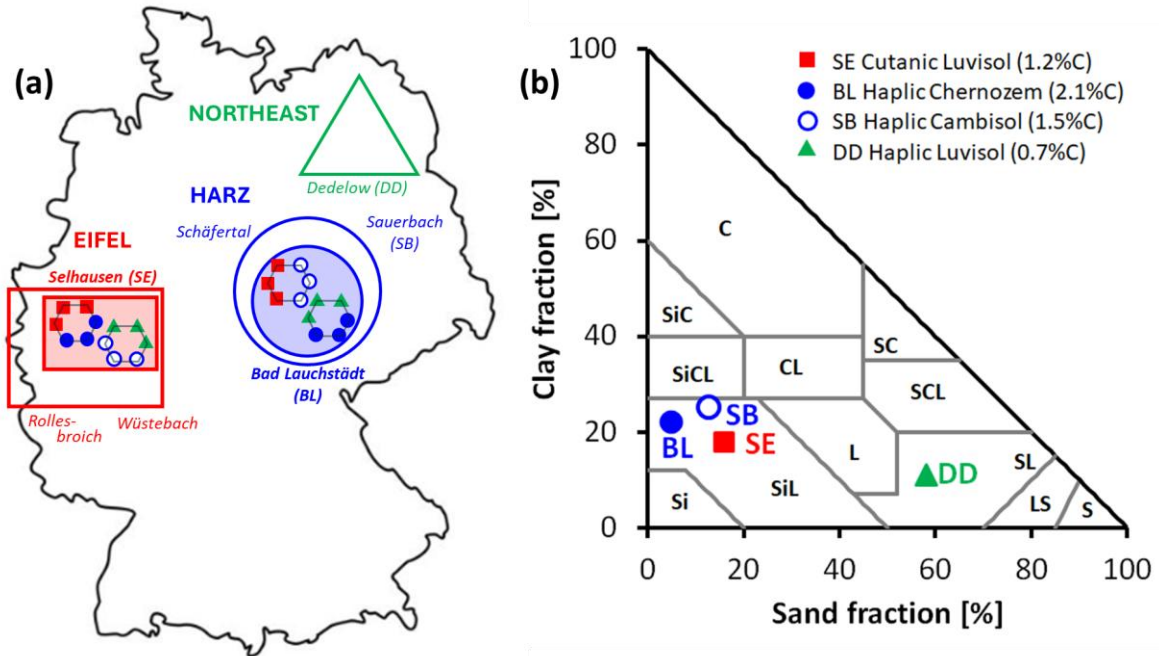
166 The input features also included a categorical moisture class (type) that reflects the expected current
167 soil water condition ('wet', 'moderate', 'dry'). This design reflects the understanding that changes in
168 climate, such as shifts in rainfall and evaporative demand, substantially affect soil water availability
169 and fluxes (Vereecken et al., 2022). The methodology is detailed in the following sections and consists
170 of six key steps: selecting study sites and datasets collected in contrasting hydro-climatic conditions
171 (subsection 2.1), preprocessing the data and extracting meaningful signal features including STL
172 (subsection 2.2), constructing and training a neural network model on a reference dataset (subsection
173 2.3), generating soil water content predictions for independent (non-training) sites using the trained
174 model (subsection 2.4), evaluating the model's performance with statistical metrics (subsection 2.5),
175 and physical consistency checks (subsection 2.6).

176 2.1 Study Sites and Data Selection

177 2.1.1 *The TERENO-SOILCan Lysimeter Network*

178 The study was conducted using lysimeter data from the TERENO-SOILCan lysimeter network in
179 Germany (Pütz et al., 2016) with a focus on two locations: Bad Lauchstädt (BL) and Selhausen (SE)
180 (Fig. 3). These sites were selected for their contrasting climatic regimes and the specific set-up of
181 lysimeters, providing a natural experiment to assess how climate variability influences soil hydrological
182 behaviour across a variety of soils. The TERENO-SOILCan lysimeters were relocated between and
183 within observatories according to a modified space-for-time approach, to expose them to different
184 climates (Groh et al., 2020). This allowed us to compare the ecosystem response of the same soil under
185 different climatic conditions. Selhausen is characterised by a humid, Atlantic-influenced climate
186 (annual precipitation around 720 mm and mean air temperature around 10 °C), whereas Bad Lauchstädt
187 represents a drier, more continental climate (annual precipitation roughly 487 mm and mean air
188 temperature approximately 8.8 °C); both climate descriptions were based on Pütz et al. (2016). Long-
189 term observations confirmed that Bad Lauchstädt experiences significantly lower rainfall and higher
190 evaporative demand than Selhausen, yielding a higher aridity index (ratio of potential
191 evapotranspiration to precipitation) and more pronounced dry spells in the growing season. By
192 including both a wetter site (Selhausen) and a drier site (Bad Lauchstädt), the model was evaluated
193 under distinctly different moisture regimes, which is critical for testing the generality of the approach
194 and distinguishing between climatic and soil type effects. For each lysimeter station (Bad Lauchstädt
195 and Selhausen), 12 lysimeters (1 m² surface area, 1.5 m depth) arranged in a hexagonal configuration
196 with 6 lysimeters around a service well were included in the analysis to monitor soil water content along
197 with meteorological variables. In this study, lysimeters were not used for drainage or storage estimates,
198 but rather as instruments providing long-term, high-resolution time series of soil water content and
199 matric potential under field conditions. The lysimeters contain undisturbed soil columns collected from
200 four different locations (see Fig. 3a), each with three replicates (Pütz et al., 2016) and are managed as
201 arable land under crop rotation. Note that all lysimeters were collected in the field and transported to
202 the lysimeter station (Pütz et al., 2016), such that no differences in packing and boundary effects are

203 expected. While fertilization practices differed regionally until spring 2019, the overall management
 204 concept was comparable, ensuring that differences in water dynamics can be attributed to changes in
 205 climate and soil rather than management (Pütz et al., 2016).



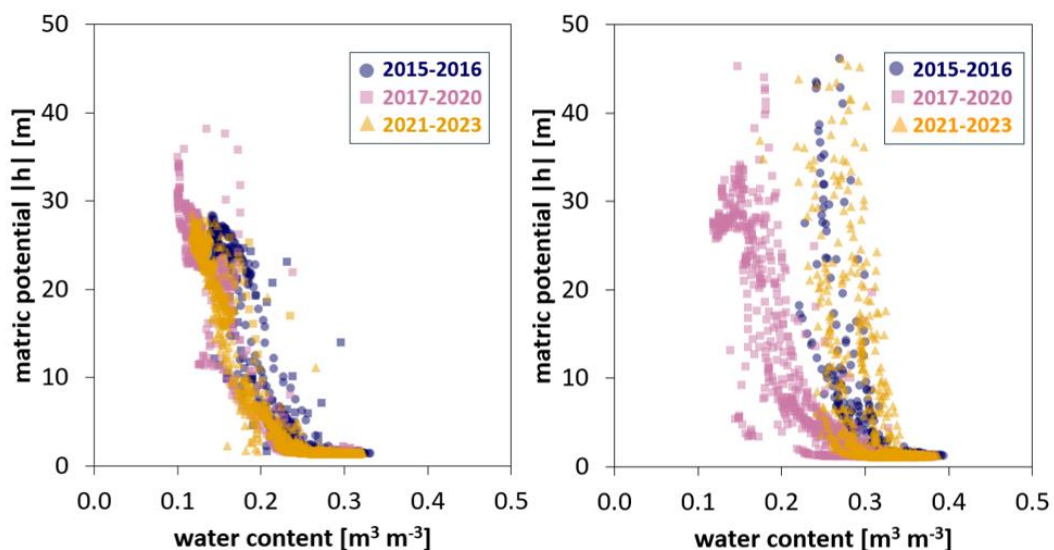
206
 207 **Figure 3** Overview of the study area with site locations, topsoil texture, and soil origin. (a) The TERENO-
 208 SOILCan network contains lysimeters from four climatic regions (different symbols and colours in the map). Our
 209 analysis focuses on the TERENO-SOILCan sites Selhausen (SE) and Bad Lauchstädt (BL), located in the
 210 Eifel/Lower Rhine Valley and Harz/Central German Lowland Observatory of TERENO, respectively, because at
 211 both sites lysimeter clusters were built (represented by shaded areas and hexagons), collecting large soil columns
 212 from four distinct source regions (i.e., Dedelow (DD), Bad Lauchstädt (BL), Sauerbach (SB), and Selhausen (SE)).
 213 (b) The analysed soil horizons (10 cm depth) cover two textural classes, shown in the USDA soil texture triangle,
 214 assigned to four different soil types and a range of soil organic carbon contents (SOC) (numbers in the legend).

215 To investigate the effects of climate on soil water dynamics, daily time series of precipitation (P),
 216 potential evapotranspiration (PET), matric potential, and volumetric soil water content (which was used
 217 as the target variable) were compiled. Precipitation at Selhausen was measured at the on-site SOILCan
 218 weather station, while for Bad Lauchstädt it was taken from the nearest long-term monitoring station
 219 operated by the Deutscher Wetterdienst (Leipzig/Halle, ID 2932; DWD Climate Data Centre, 2025).
 220 PET was calculated with the FAO-56 Penman–Monteith model (Allen et al., 2006), using measured
 221 meteorological variables (air temperature, air pressure, relative humidity, radiation, and wind speed)
 222 according to SOILCan protocols (Pütz et al., 2016; Groh et al., 2020). In this context, the reference
 223 evapotranspiration (ET_o) calculated with the Penman–Monteith model for a clipped grass surface

224 (FAO-56) was used as a proxy for potential evapotranspiration (PET), representing the site-independent
 225 atmospheric evaporative demand. Soil matric potential was measured using MPS-1 sensors (Decagon
 226 Devices Inc., Pullman, WA, USA), and volumetric soil water content was measured with time-domain
 227 reflectometry probes (CS610, Campbell Scientific, North Logan, UT, USA). The observational record
 228 spans the period from 2014 to 2023 and includes measurements taken at a depth of 10 cm (deeper soil
 229 layers were not analysed; Pütz et al., 2016).

230 2.1.2 Definition of Reference Site for Model Framework

231 For model development, a single lysimeter moved from Dedelow to the Bad Lauchstädt lysimeter
 232 station (see Fig. 3a and 3b) was selected as the training dataset. This lysimeter was chosen due to its
 233 stable soil water content dynamics and minimal temporal drift in water retention properties over the
 234 observation period (see Fig. 4a). This lysimeter served as the reference dataset for developing the
 235 predictive model because it allows the definition of the soil water content response function for seasonal
 236 climatic conditions. The 23 remaining lysimeters at the Bad Lauchstädt and Selhausen sites were used
 237 as independent test datasets (a contrasting example is shown in Fig. 4b) to evaluate model generalisation
 238 and detect potential shifts in soil hydraulic behaviour across sites and years.



239 **Figure 4** Soil water retention curves using data collected between 2015 and 2023 at 10 cm depth. Matric potential
 240 is plotted against volumetric water content, with data colour-coded by period: 2015–2016 (blue), 2017–2020
 241 (green), and 2021–2023 (red). (a) Training lysimeter (moved from Dedelow to Bad Lauchstädt). (b) Test lysimeter
 242 (original soil from Selhausen in lysimeter station at Selhausen).
 243

244 2.2 Data Preprocessing and Feature Engineering

245 All raw data were aggregated or resampled to a daily time step to support time-series analysis and
246 modelling. Any misaligned or duplicated timestamps were corrected to ensure consistency.
247 Measurements before 2015 were excluded from both sites to allow sensor settlement after installation.

248 *2.2.1 Seasonal-Trend decomposition*

249 To provide the model with structured representations of climate variability, each climatic time series
250 was decomposed into additive components using STL (Seasonal–Trend decomposition based on
251 LOESS, a locally weighted regression method) (Cleveland et al., 1990). STL is a non-parametric
252 method that separates a time series into three interpretable components: a seasonal component
253 representing repeating seasonal patterns (such as wetting and drying cycles), a trend component
254 capturing gradual long-term changes (such as climate shifts), and a residual component containing
255 short-term irregularities and high-frequency noise (Cleveland et al., 1990). This decomposition was
256 applied independently to the P, PET, and WB time series. Only the seasonal and trend components were
257 retained as input features, as they contain meaningful patterns relevant to soil water content dynamics.
258 The residual component, which lacks a systematic structure, was excluded from further analysis. STL
259 was configured with a cycle length of 180 days, representing the semi-annual wet–dry phases at the
260 study sites. A LOESS smoother with a 90-day window was then applied to the de-seasonalized series
261 to extract the trend component. This configuration was chosen to capture gradual, long-term changes in
262 the climatic variables while reducing short-term fluctuations. However, near the ends of the time series,
263 the absence of future values causes the smoothing window to become asymmetric. As a result, the
264 estimated trend becomes more sensitive to recent variability. This limitation does not affect the outcome
265 of the analysis, as both the input features and the target variable (water content) are equally influenced
266 by it. Each of the extracted seasonal and trend components from P, PET, and WB was included as input
267 to the neural network alongside the original raw values. This allowed the model to learn structured
268 seasonal behaviour—such as distinguishing the rising phase of spring wetting up of the soil profile from
269 the declining phase of a summer dry-down—and to account for long-term shifts, such as gradual drying
270 or changes in mean climate conditions.

271 2.2.2 *Wetness classification*

272 In addition to the continuous climate-related features, a categorical input was included to describe the
273 soil moisture condition as either ‘dry’, ‘moderate’, or ‘wet’. These categories were defined using the
274 soil water content time series from the training site, with thresholds based on quantiles of the full
275 distribution. Specifically, values below the 30th percentile were labelled as ‘dry’, between the 30th and
276 70th percentiles as ‘moderate’, and above the 70th percentile as ‘wet’. These categories were encoded
277 numerically prior to modelling, using values of 30 for ‘dry’, 20 for ‘moderate’, and 1 for ‘wet’ (higher
278 values correspond to drier conditions). This encoding allowed the categorical feature to be treated as an
279 ordinal variable and integrated into the neural network input layer alongside the other features. The
280 thresholds were selected to provide clear regime separation while ensuring sufficient observations per
281 class for robust model training.

282 There were two reasons for including this feature. First, the soil’s current moisture condition can
283 strongly influence its response to P and PET (Western & Grayson, 1998). For example, under dry
284 conditions, more water can be absorbed by the soil due to its high storage capacity. In contrast, when
285 soils are already wet or near saturation, infiltration capacity is reduced, and additional rainfall is more
286 likely to result in runoff (Tromp-van Meerveld & McDonnell, 2006; Zehe & Blöschl, 2004). The second
287 reason is the motivation to use remote sensing data in similar follow-up studies, which are not yet
288 accurate enough for modelling purposes but allow a general classification of the wetness status. Because
289 (i) corresponding information on soil matric potential cannot be deduced at larger scales from remote
290 sensing data and (ii) hysteresis in the soil water retention curve may lead to ambiguous thresholds, we
291 focus here on soil water content measurements.

292 Another aspect of the model framework that must be discussed is the selection of the percentile
293 thresholds. From a soil hydrological point of view, it would make sense that the thresholds defining the
294 three classes ‘wet’, ‘moderate’, and ‘dry’ are chosen individually for each lysimeter (a wet clay soil
295 may have very different water content values than a sandy soil). However, from a methodological point
296 of view, we prefer to ensure that the model does not require a long time series to determine quantiles of
297 soil water content data and that it can be applied solely based on the training site’s distribution.

298 Accordingly, the same percentile thresholds, derived from the training site, were applied to label daily
299 water content values at the prediction sites. Note that applying the same percentile thresholds for all
300 sites does not affect the detection of changes in the soil water content response function. Very similar
301 results were obtained for a site-specific percentile definition as shown in the supplementary material
302 (Section S1). After constructing all the above features, each daily input to the model consisted of (i)
303 raw climate variables (P, PET, and WB), (ii) the STL-derived seasonal and trend components for each
304 variable (six variables), and (iii) the categorical moisture label. All ten features were aligned by date to
305 ensure consistency across inputs. This combination of raw values, decomposed temporal signals, and
306 qualitative soil condition provided the model with a detailed daily representation of both external
307 climatic forcing and internal system state.

308 2.3 Neural Network Architecture and Training

309 To model daily volumetric soil water content, a feed-forward neural network was implemented. The
310 architecture consisted of three hidden layers: two dense layers with 12 neurons each using ReLU
311 activation functions (Rectified Linear Units), followed by a batch normalization layer, and a third dense
312 layer with 6 neurons. ReLU was chosen for its ability to introduce non-linearity while maintaining
313 computational efficiency and avoiding vanishing gradient problems during training (Lu et al., 2020;
314 Montesinos López et al., 2022). Batch normalization was applied to stabilize learning by reducing
315 internal covariate shift, which improves convergence speed and training stability (Montesinos López et
316 al., 2022). The output layer consisted of a single neuron with a linear activation function, which is
317 standard for continuous regression tasks such as predicting soil water content.

318 The network was trained using input features derived from daily observations at the reference lysimeter
319 at the Bad Lauchstädt site, covering the period 2015–2023. Prior to training, all continuous input
320 features were standardized to have a mean of zero and a standard deviation of one using z-score
321 normalization. The standardization parameters (mean and standard deviation) were computed solely
322 from the training dataset and applied unchanged to the validation and test sets at the training site, as
323 well as to the prediction sites, ensuring consistency across all data splits. The target variable, volumetric
324 soil water content, was preserved in its original physical units ($\text{m}^3 \text{m}^{-3}$), allowing for direct interpretation

325 of the model outputs and associated errors in hydrologically meaningful terms. The model was compiled
326 with the Adam optimizer, which adaptively adjusts learning rates and is widely used for its
327 computational efficiency and stable convergence (Kingma and Ba, 2015). Mean squared error (MSE)
328 was used as the loss function due to its sensitivity to large deviations, making it suitable for continuous
329 regression tasks. To monitor generalisation, 30% of the data were withheld as a validation set and
330 excluded from updating the weights between the nodes during training. The training procedure was
331 initially set to proceed for a maximum of 1000 epochs. To prevent overfitting, an early stopping
332 criterion was implemented based on validation loss. Specifically, training was terminated if no
333 improvement in validation performance was observed over a predefined number of consecutive epochs
334 (patience threshold). The model parameters from the epoch exhibiting the lowest validation loss were
335 retained for final evaluation.

336 2.4 Testing the Neural Network

337 After training, the model was applied to the remaining 23 lysimeters across both Selhausen and Bad
338 Lauchstädt, none of which were included in the training phase. All test inputs were processed using the
339 same structure and normalization parameters derived from the training data. As outlined in Section 2.1,
340 the experimental setup includes four soil types, each installed with three replicates at both sites (see Fig.
341 3). While the lysimeters at the Bad Lauchstädt station share the same climatic setting as the training
342 site, the lysimeters at Selhausen represent a more humid region. Accordingly, the raw data and STL-
343 derived seasonal and trend components of the Selhausen climate were used as input for the prediction
344 of soil water content in lysimeters located at Selhausen. This configuration allows for the evaluation of
345 (i) whether the soil water content response function determined for the training site remains valid across
346 different climates and soil types, and (ii) the detection of potential temporal changes in soil hydraulic
347 behaviour. The evaluation and classification procedures are described in the following two subsections.

348 2.5 Detection of Change in Soil Water Content Response Function Based on Error 349 Metrics

350 As explained in the introduction, we use error metrics to detect changes in the soil water content
351 response function. While we use the Nash–Sutcliffe efficiency (NSE; see Eq. 5) as a general descriptor

352 of model error, we investigate temporal changes in model performance based on the Mean Bias (MB)
353 that was calculated on an annual basis from 2015 to 2023. This year-by-year assessment does not rely
354 on predefined change points and enables the detection of gradual or abrupt shifts in model performance
355 directly from the data. MB measures the average signed difference between predicted and observed
356 values, providing an estimate of systematic overestimation or underestimation over time (Moriassi et al.,
357 2007; Liu et al., 2011), and is defined as:

$$358 \quad MB = \frac{1}{N} \sum_{i=1}^N (\hat{\theta}_i - \theta_i) \quad (1)$$

359 where $\hat{\theta}_i$ is the predicted volumetric water content at day i , θ_i is the corresponding observation, and N
360 defines the number of available observations–prediction pairs. Although the calculation uses daily
361 values, MB was aggregated over yearly intervals to produce a single value per year, capturing annual
362 patterns in prediction bias. Volumetric water content ($\text{m}^3 \text{ m}^{-3}$) was multiplied by 100 prior to
363 calculation, and MB is therefore reported in percentage (%). Positive MB values indicate systematic
364 overestimation by the model, while negative values reflect underestimation. The annual assessment of
365 MB allowed us to evaluate whether the soil water content response function remains consistent over
366 time or shows temporal dynamics. Deviations between predicted and observed water content can differ
367 in sign across moisture conditions and event types, such that opposite errors may partially cancel when
368 averaged over a full year. Therefore, mean bias is interpreted as an indicator of long-term temporal drift
369 in model–observation differences, while soil water retention curves are used here (see next section) to
370 verify the physical consistency and direction of detected changes; in cases where retention
371 measurements are not available, robustness of bias trends can alternatively be assessed by repeating the
372 analysis using different temporal aggregation periods.

373 To classify the soil water content dynamics with respect to the resilience after the extreme summer of
374 2018, we checked if the deviation of the predictions based on a stable response function (developed
375 using the training data) changed over the years. When the deviation in the first year (2015; i.e., before
376 the drought) is different from the deviation in the year 2023, we consider that the soil water content
377 response function has changed (it is still possible that the response function may recover in the future)
378 and the state of the soil water content dynamics is classified accordingly as being ‘changed’. When the

379 deviations at the beginning and end are similar, but there was a period between 2018 and 2022 with a
 380 different deviation level, we conclude that the soil water content response function changed reversibly
 381 over time but recovered within the observation window and the lysimeter is classified as ‘resilient’.
 382 Note that in resilience-related literature, the system response to disturbance is often characterised by
 383 the time scale and rate of recovery following perturbation (Scheffer et al., 2009). Here, we do not
 384 analyse the recovery period in more detail, but based on the definition of the ‘resilient’ category,
 385 recovery must occur within four years.

386 The soil water content response is considered as ‘stable’ when the deviations remain similar during the
 387 entire observation period (i.e., the same response function of soil moisture dynamics to climatic
 388 conditions can be used). As a threshold, we chose 1.52%, which equals the 3-fold of the standard
 389 deviation of the nine yearly MB values computed for the training site. The classification of the time
 390 series was thus expressed formally as:

391 ‘changed’: $|MB_{2023} - MB_{2015}| > 1.52\%$ (2)

392 ‘resilient’: $|MB_{2023} - MB_{2015}| \leq 1.52\% \wedge |MB_{20xx} - MB_{2015}| > 1.52\%$ (3)

393 ‘stable’: $|MB_{2023} - MB_{2015}| \leq 1.52\% \wedge |MB_{20xx} - MB_{2015}| \leq 1.52\%$ (4)

394 with the logical operator \wedge and the mean bias of a specific year denoted as MB_{20xx} , which shows the
 395 largest difference $|MB_{\text{year}} - MB_{2015}|$ for the period between 2018 and 2022 (starting with the dry year
 396 2018).

397 As general information on the different response functions, we calculated the Nash–Sutcliffe efficiency
 398 (NSE) coefficient (Moriassi et al., 2007; Nash & Sutcliffe, 1970). The NSE is a standard metric for
 399 hydrological model skill, with $NSE = 1$ indicating perfect agreement and $NSE \leq 0$, indicating that the
 400 model predictions are no better than using the mean of the observations. Mathematically, it is defined
 401 as:

402
$$NSE = 1 - \frac{\sum_{i=1}^N (\theta_i - \hat{\theta}_i)^2}{\sum_{i=1}^N (\theta_i - \bar{\theta})^2}$$
 (5)

403 where $\hat{\theta}_i$ is the predicted volumetric water content at day i , θ_i is the corresponding observed value, $\bar{\theta}$ is
404 the mean observed volumetric water content over the evaluation period, and N denotes the total number
405 of valid data points used in the calculation. Following Moriasi et al. (2015), model performance was
406 classified as very good for $NSE > 0.80$, good for $0.70 < NSE \leq 0.80$, satisfactory for $0.50 < NSE \leq 0.70$,
407 and unsatisfactory for $NSE \leq 0.50$.

408 In this study, NSE is used to summarize the overall agreement between simulated and observed soil
409 water dynamics, whereas the identification and classification of temporal changes in the soil water
410 content response function rely exclusively on the annual evolution of mean bias. Lower NSE values
411 were interpreted as reduced dynamic agreement between the tested lysimeter and the reference soil–
412 climate response used for training, without implying a specific mechanism of change.

413 2.6 Interpretation of Change in Response Function in Soil Physical Terms

414 The dynamics of MB (see above) were also used to assess changes in soil water retention curves
415 (SWRCs), which were plotted for each test lysimeter on a yearly basis. As stated in Eq. (1), a positive
416 MB value corresponds to measured water content values that are smaller than the predictions. Because
417 the predictions are based on the model trained for a specific lysimeter, we expect that, for a positive
418 MB, the water content for the same environmental conditions (as manifested in the matric potential) is
419 smaller in the test lysimeter compared to the lysimeter used for training (SWRC is shifted to the left).
420 Similarly, a consistently negative MB suggests that the test site may retain more water at a given matric
421 potential than the training site, and that the SWRC is likely shifted to the right. For a ‘resilient’ soil, the
422 soil water retention curve shifts back close to the original position at the end of the observation period.
423 Finally, for a soil with a ‘changed’ response function, the water retention curve drifts over time, but
424 without returning to its original position. In some cases, the temporal evolution of MB may not exactly
425 follow the apparent shift of the SWRC, as additional vertical or slope changes could occur due to
426 variations in porosity or pore-size distribution. These effects cannot be identified within the current
427 framework but may contribute to deviations between MB dynamics and the apparent SWRC shift. To
428 further support the SWRC-based interpretation, a quantitative analysis of soil water retention curve

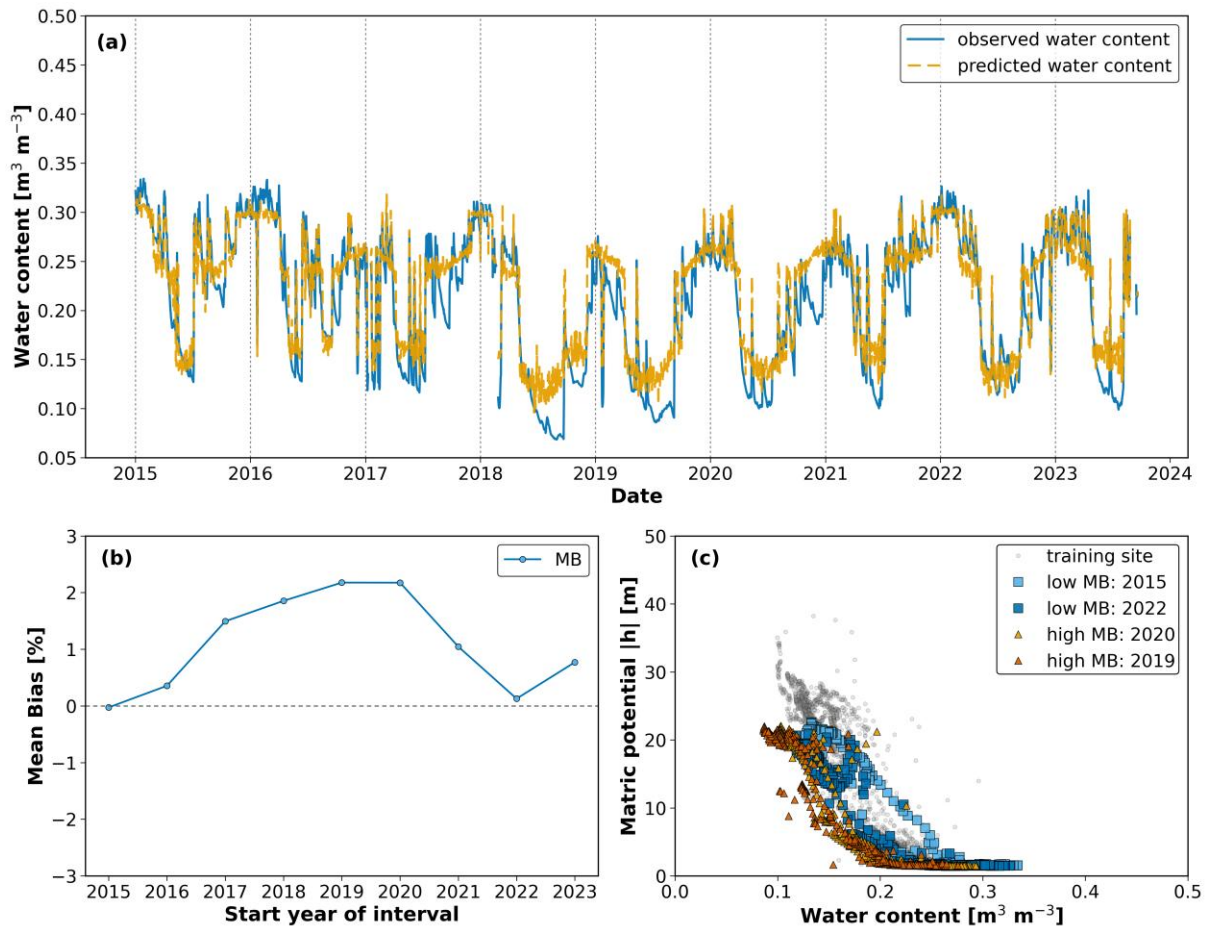
429 evolution based on the concept of integral mean water content is provided in the Supplementary
430 Material.

431 3. Results

432 Following the methodological framework described in Sections 2.3–2.6, we present the model
433 predictions across the test lysimeters to assess the resilience of the soil water content response function
434 for the different lysimeters. We organise the section in four subsections according to the four different
435 origins of the soil in the lysimeters (see Fig. 3b) to discuss effects of soil origin and climatic conditions
436 on the response function. In the last subsection (3.5), the results are summarized to allow direct
437 comparison of all 24 lysimeters. Note that all model results presented below are based on the soil water
438 content classification (‘wet’, ‘moderate’, ‘dry’) as deduced from the lysimeter used for model training.
439 The corresponding figures using a site-specific classification for each lysimeter are shown in
440 Supplementary Information Fig. S4–S7.

441 3.1 Lysimeters with same soil as used in model training (Dedelow soils)

442 The neural network was trained to capture the soil water content response function of one lysimeter
443 with sandy loam topsoil (Luvisol) extracted from Dedelow and translocated to the dry climatic region
444 in Bad Lauchstädt (see Fig. S1 in the Supplementary Material). The NSE of the training and validation
445 for that specific lysimeter was very high, with a value of 0.91, indicating good model performance. The
446 application of this response function to the other two lysimeters from Dedelow that were translocated
447 to Bad Lauchstädt resulted in relatively high NSE values (0.79 and 0.84), but the response in summer
448 2018, characterised by lower soil water content, was not captured accurately (Fig. 5a). More
449 specifically, the time series showed that predictions and observations matched closely in 2015, while
450 after the dry summer of 2018 the model systematically overestimated water content in 2019 and 2020,
451 before the agreement improved again towards the end of the period.



452
 453 **Figure 5** Analysis of soil water content dynamics (2015–2023) for a Dedelow-origin lysimeter tested at Bad
 454 Lauchstädt. Panel (a) shows the time series of observed (blue) and predicted (orange) water content, with close
 455 agreement in 2015, clear overestimation in 2019–2020 (predictions above observations), and improved
 456 agreement again towards the end of the period. Panel (b) presents the temporal evolution of mean bias (MB),
 457 remaining near zero until 2017, increasing to about 2–3 % in 2019–2020, and decreasing again to approximately
 458 zero in 2022. Such soil water content response was classified as ‘resilient’. Panel (c) displays soil water retention
 459 curves from the training site (grey) and from selected years representing different MB conditions, with low-MB
 460 years (2015, 2022) and high-MB years (2019, 2020). The curves are close to the training site in 2015, show a
 461 shift to lower water contents in 2019–2020, and in 2022 return to the training site data.

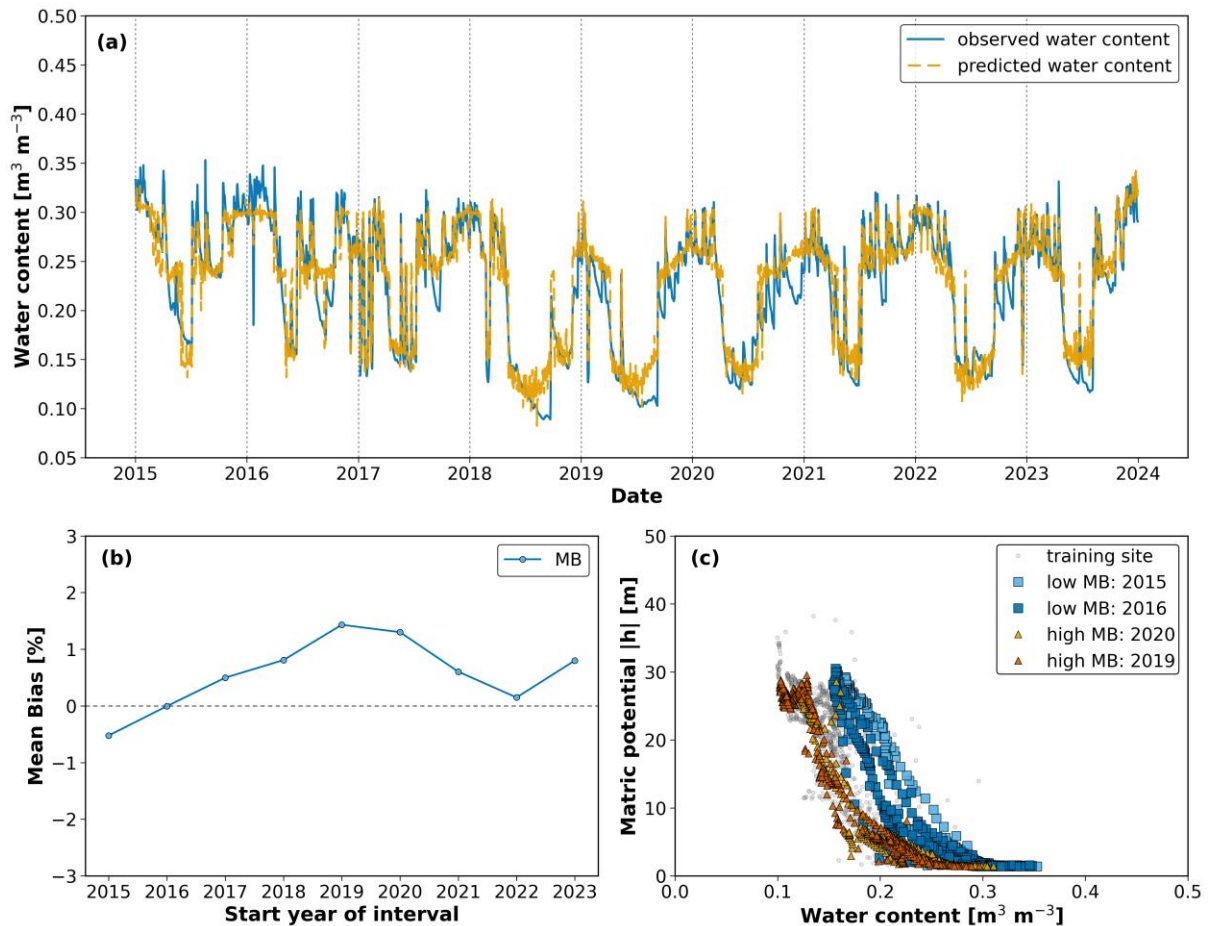
462 These changes are reflected in the MB trend development (Fig. 5b), with values increasing from near
 463 zero in 2015 to about 2–3% in 2019–2020 and then decreasing again towards 2022. The retention curves
 464 confirm this interpretation (Fig. 5c). The year with low MB (2015) produced a SWRC close to the
 465 measured curve of the training site; the years with high MB (2019–2020) were shifted towards lower
 466 water contents, and the later year with reduced MB (2022) returned to the measured SWRC of the
 467 training site. Taken together, the time series, MB trend, and SWRCs show that the soil response was
 468 disturbed after 2018 but later recovered, which classifies this lysimeter as ‘resilient’. The same finding

469 holds for the simulations of the lysimeters translocated to Selhausen (less dry climate) with high NSE
470 between 0.80 and 0.82. This indicates that for the coarse-textured soil included in this study (i) the effect
471 of changing climatic conditions was rather small (very good NSE classification for both sites), but (ii)
472 that these coarse-textured topsoils do not show identical responses to the extreme year, as each lysimeter
473 reacts slightly differently, which may indicate small differences in hydraulic properties.

474 3.2 Lysimeters with soils formed under the same climate as the one used in model 475 training (Bad Lauchstädt soil)

476 The lysimeters filled with soil from Bad Lauchstädt (Chernozem) were formed under the climatic
477 conditions used for fitting the response function. In the case of a dominant effect of climate on the soil
478 water content response function, we could expect similar results as for the training lysimeter. For the
479 soil remaining at the original site (Bad Lauchstädt), the model performance was very good (0.88–0.89).
480 As shown for example in Fig. 6a, the fit between observed and predicted water content was consistently
481 close, with a tendency to slightly underestimate in the early years and to mildly overestimate after 2018,
482 particularly in 2019–2020, before the agreement improved again in later years. This is also manifested
483 in the MB values that increased from slightly negative values in 2015 to about +1.5% in 2019, before
484 decreasing again towards zero (Fig. 6b). The plotted SWRCs support this interpretation (Fig. 6c), with
485 low MB years (2015 and 2016) showing a slight shift towards higher water contents relative to the
486 measured SWRC of the training site, and high-MB years (2019 and 2020) displaying a modest shift
487 towards lower water contents. Accordingly, the state of the soil water content dynamics was classified
488 as ‘resilient’.

489 For the lysimeters transported from Bad Lauchstädt to Selhausen, the performance was more variable
490 (NSE ranging from 0.50 to 0.84), corresponding to classifications ranging from satisfactory to very
491 good, reflecting the stronger effect of the wetter climate. None of the three lysimeters that stayed in Bad
492 Lauchstädt were classified as ‘changed’, but two out of three showed a systematic shift and were
493 classified as ‘changed’ when translocated to Selhausen (see Table 1). In short, these examples show
494 that the Bad Lauchstädt soil remained resilient under its original climatic conditions at Bad Lauchstädt
495 but changed when exposed to the wetter climatic conditions at Selhausen.

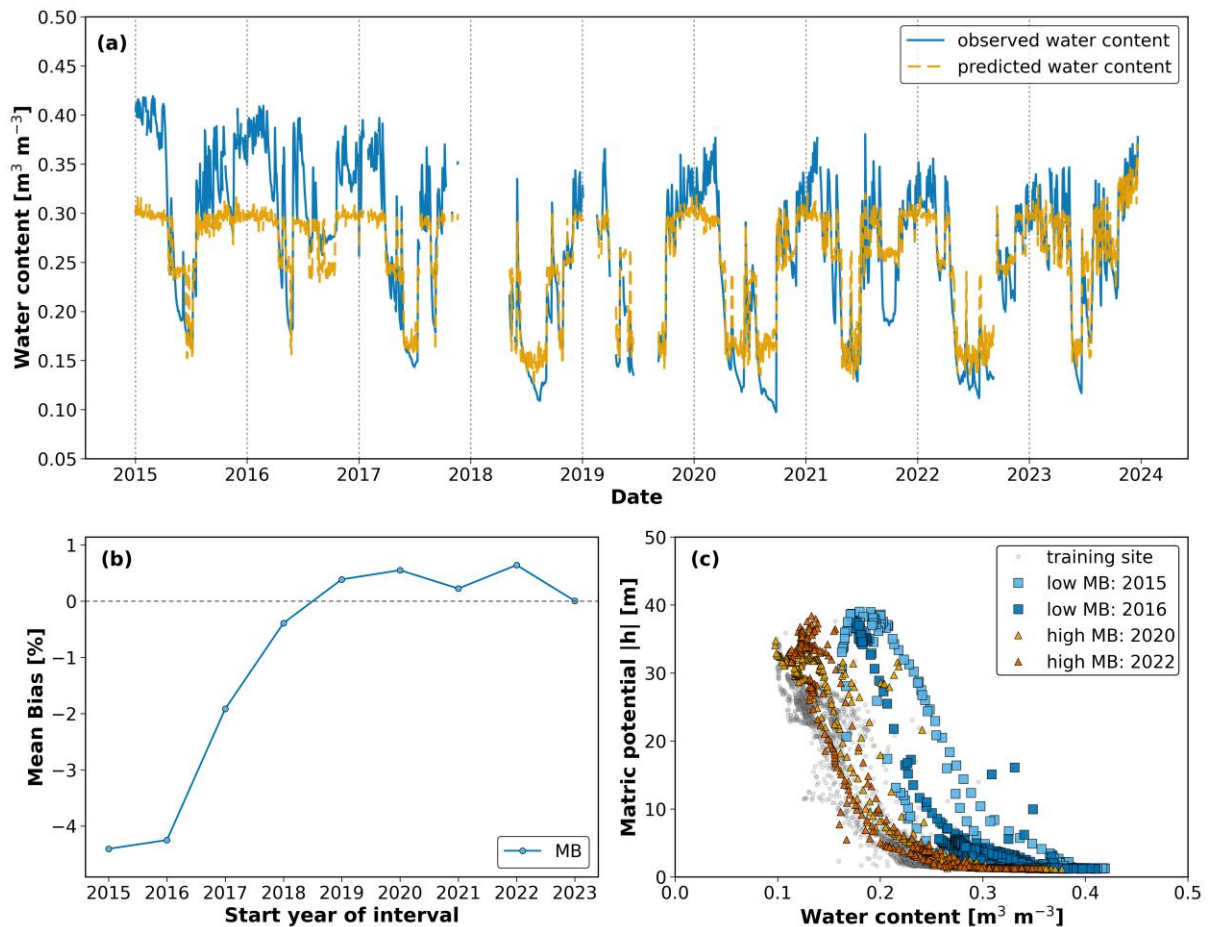


496
 497 **Figure 6** Analysis of soil water content dynamics (2015–2023) for a Bad Lauchstädt-origin soil lysimeter tested
 498 at Bad Lauchstädt. (a) Comparison of measured (blue) and simulated (orange) daily water content values,
 499 showing high agreement in the early years and temporary overestimation in 2019–2020. (b) Mean Bias (MB)
 500 started slightly negative in 2015, increased to about +1.5 % in 2019, and then decreased again towards 2022. (c)
 501 Soil water retention curves (SWRCs) from the training site (grey) and from the same replicate for selected years
 502 with low MB (2015, 2016) and high MB (2019, 2020) show close agreement in the early years and a shift to lower
 503 water contents in 2019–2020.

504 3.3 Lysimeters with soils formed under a similar climate to the one used in model 505 training (Sauerbach soil)

506 The findings are similar for the silt loam (Cambisol) from Sauerbach that was formed under climatic
 507 conditions similar to those in Bad Lauchstädt. As in the case of the soil from Bad Lauchstädt, soils from
 508 Sauerbach show higher NSE values when translocated to Bad Lauchstädt (0.81–0.88, very good)
 509 compared to those transferred to the wetter climate in Selhausen (0.74–0.79, good). This reflects that
 510 the soil water content response function in the drier climate is not the same as in the wetter climate. In
 511 one illustrative case, the observed water content initially showed wetter dynamics than predicted, but

512 gradually converged towards the model predictions by 2023, indicating a possible adjustment in soil
 513 hydraulic response over time (Fig. 7a).



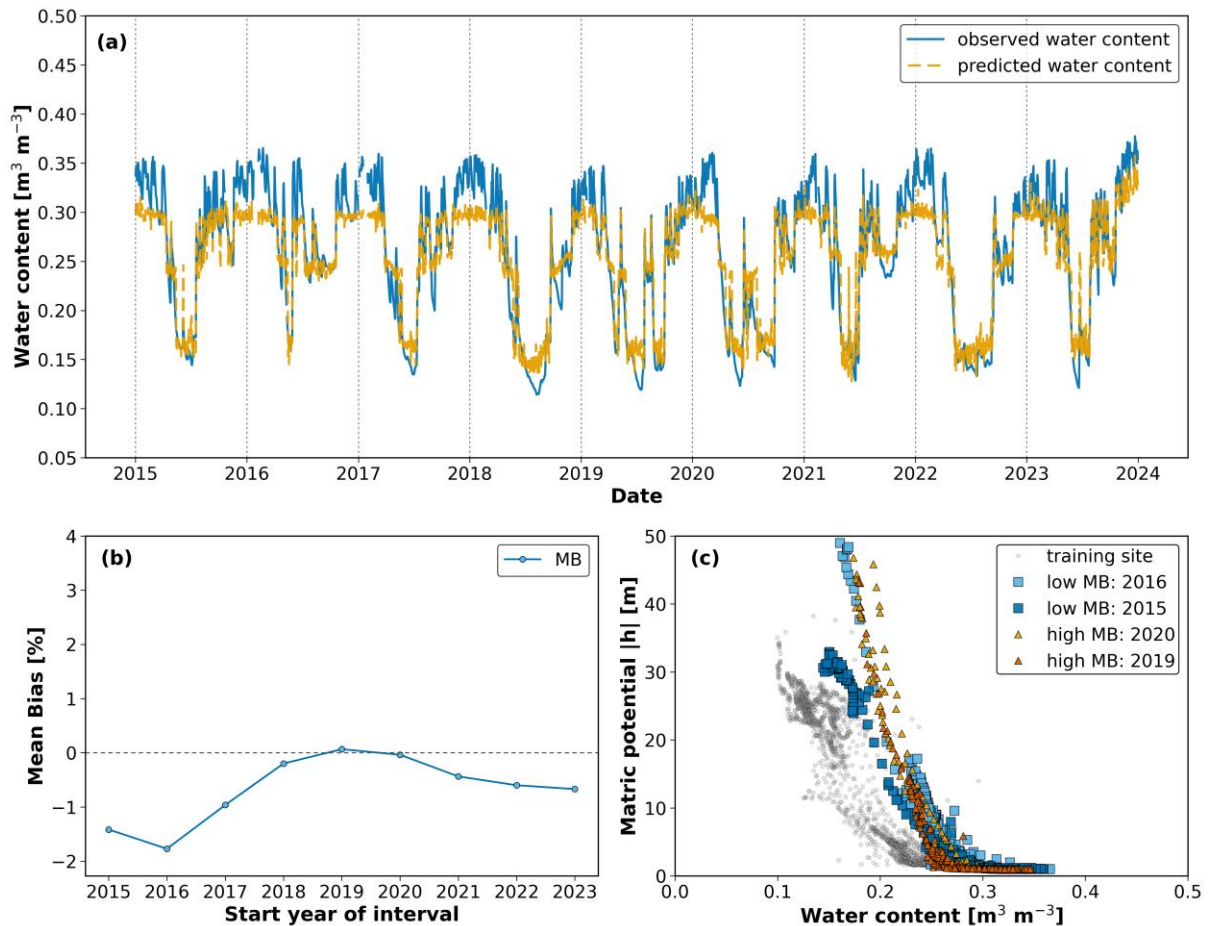
514 **Figure 7** Analysis of soil water content dynamics (2015–2023) for Sauerbach-origin lysimeter relocated to
 515 Selhausen (a) Comparison of observed and predicted daily volumetric water content ($NSE = 0.74$); Ater initial
 516 underestimation by the model, the observed and predicted values gradually converged, indicating a possible
 517 adjustment in soil hydraulic behaviour over time. (b) Temporal evolution of the mean bias (MB), which increased
 518 from about -5% in 2015 to values close to zero by 2019–2023, consistent with the improved match between
 519 observed and predicted values shown in panel (a). (c) Soil water retention curves (SWRCs) from the training site
 520 (grey) and from selected years with low MB (2015, 2016) and high MB (2020, 2022) illustrate the same trend,
 521 with early years showing higher water contents at a given matric potential and later years shifting towards the
 522 training curve.
 523

524 This development is also evident in the MB values (Fig. 7b), which started strongly negative (-5%) in
 525 2015–2016 and steadily increased towards values close to zero by 2023, indicating a progressive
 526 reduction in underestimation. The corresponding SWRCs (Fig. 7c) confirm this trend, with curves from
 527 early years (2015, 2016) showing higher water contents at a given matric potential compared to the
 528 measured SWRC of the training site, while later years (2021, 2023) shifted closer to the reference,

529 suggesting a gradual adjustment of hydraulic behaviour. In the case of soils from Sauerbach, there was
530 a difference in the quantification of resilience with respect to the classification of the soil water content
531 used as an input variable: with the classification based on the training lysimeter (with sandy loam in the
532 topsoil), the soil water content dynamics were classified as ‘changed’ for all six lysimeters. However,
533 using the classification based on the soil water content statistics obtained for each lysimeter individually
534 (see Fig. S6), the high water contents at the beginning were better captured, and only one lysimeter out
535 of three was classified as ‘changed’. Independent of the water content classification, all lysimeters
536 translocated to Selhausen were classified as ‘changed’, exhibiting the strongest response to relocation
537 among all soils.

538 3.4 Lysimeters with soils formed under a different climate compared to the one 539 used in model training (Selhausen)

540 Finally, we discuss the Selhausen silt loam (Luvisol), which was formed under climatic conditions that
541 were not used in the training of the neural network. The model performance was better for the replicates
542 translocated to the drier Bad Lauchstädt climate (NSE = 0.86–0.92, very good), compared to slightly
543 lower performance at their site of origin under humid Atlantic conditions (0.76–0.86, good to very
544 good). The classification with respect to resilience helps to explain this, since Selhausen soils at their
545 origin were mainly assigned to ‘stable’ or ‘resilient’ categories (see Table 1), while the same soils
546 translocated to Bad Lauchstädt showed a more variable pattern. This indicates that the lower NSE at
547 Selhausen does not represent a misfit of the model but reflects that the soils follow their own stable soil
548 water content response function. One replicate at Selhausen (NSE = 0.85) reproduced the seasonal
549 dynamics well, although differences between observed and predicted values remained visible in the wet
550 season across several years (Fig. 8a). The MB shifted from negative values in the first years towards
551 zero after 2019. Note that an MB value of 0 does not mean that deviations disappeared, but that errors
552 in wetter and drier phases compensated each other (Fig. 8b). The SWRCs were generally close to the
553 training reference, but in later years, small deviations appeared mainly at the saturated end (Fig. 8c).
554 Overall, these changes remained below the assumed threshold, supporting the classification of the soil
555 water content dynamics as ‘stable’.

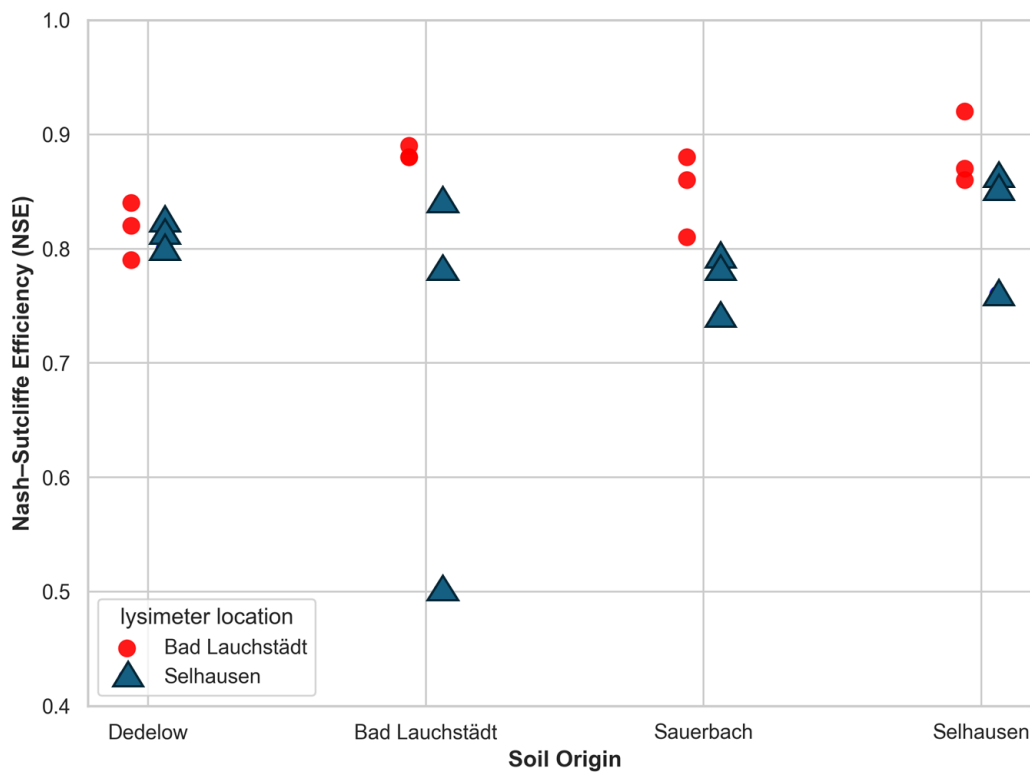


556
 557 **Figure 8** Soil water content dynamics (2015–2023) for a Selhausen-origin lysimeter tested at Selhausen. (a)
 558 Observed (blue) and predicted (orange) water content shows fair agreement, with underestimation of water
 559 contents in the wet season. (b) Mean Bias (MB) fluctuated from negative values in the early years to values close
 560 to zero after 2019, but these variations remained below the threshold for change. (c) Soil water retention curves
 561 (SWRCs) from the training site (grey) and from selected years with low MB (2015, 2016) and higher MB (2019,
 562 2020) reflect these minor variations, with the 2019 curve showing the strongest deviation yet remaining close to
 563 the training reference, consistent with the stable classification. The apparent cutoff at the wet end in (a) arises
 564 from the use of absolute rather than normalized values during training, as discussed in the Supplementary
 565 Material (Text S1).

566 3.5 Comparison of all lysimeters

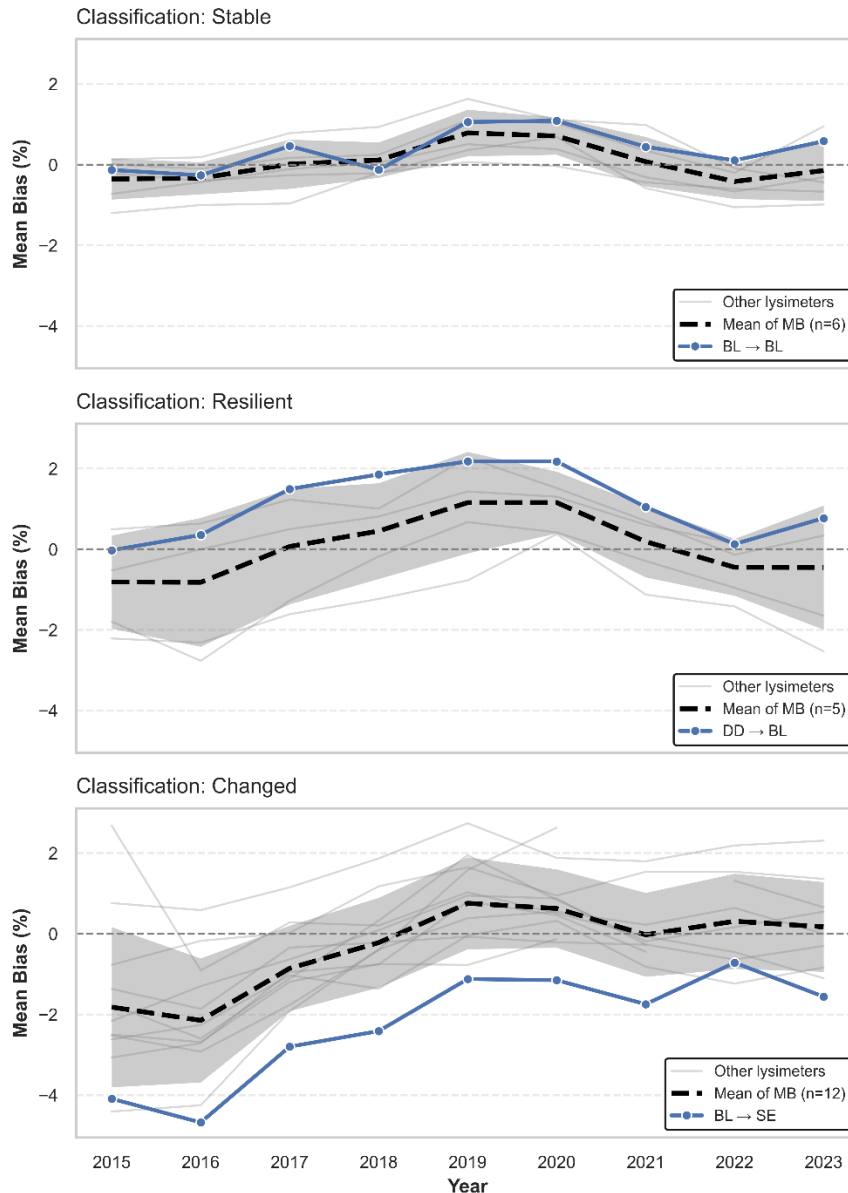
567 The comparison of the soil water content dynamics of all lysimeters indicates that contrasting climatic
 568 conditions between sites — particularly between the continental Bad Lauchstädt and Atlantic-
 569 influenced Selhausen — can significantly alter the hydraulic response of the soil, even when texture
 570 remains constant. In general, prediction performance at Selhausen was lower, likely because the model
 571 was trained under the drier climate of Bad Lauchstädt and therefore failed to fully capture the soil–

572 water interactions emerging under wetter conditions (Fig. 9). The broader NSE range observed at the
 573 Selhausen location further suggests increased variability in hydraulic response among replicates.



574 **Figure 9** Spread of Nash–Sutcliffe efficiency (NSE) values across different soil origins and test locations. Each
 575 symbol represents one lysimeter from a given origin (x-axis) evaluated at Bad Lauchstädt or Selhausen (indicated
 576 by colour). The results highlight the influence of climate–soil interactions on model performance. Notably, Bad
 577 Lauchstädt-origin soils exhibited strong performance at their origin but a wider and lower range when tested at
 578 Selhausen, indicating increased variability in soil hydraulic behaviour and divergence in soil–climate response.
 579

580 With respect to resilience of the soil water content response function, we show the temporal evolution
 581 of the mean bias for all lysimeters in Fig. 10 and summarize the results in Table 1. In Table 1 we include
 582 the general classification type (‘stable’, ‘resilient’ and ‘changed’) and calculate the average of three
 583 lysimeters (same material and same location) for (i) the drift in mean bias value between the year 2015
 584 and 2023 and (ii) the maximum deviation from 2015 for the years between 2018 and 2022. The table
 585 shows that deviations from a ‘stable’ or ‘resilient’ response function mainly occur when soils from
 586 Dedelow, Bad Lauchstädt, and Sauerbach were translocated to Selhausen. Only in the case of the soil
 587 from Selhausen, the response function remains ‘stable’. It seems that the soil material ‘trained over
 588 decades’ to the wetter climate in Selhausen adapts better to the extreme summer 2018.



589
590 **Figure 10** Temporal evolution of Mean Bias (MB) for three representative lysimeter replicates, each classified
591 into one of three soil hydraulic response categories: (a) ‘stable’, (b) ‘resilient’, and (c) ‘changed’. Thick dashed
592 lines indicate the mean of the MB trend across all lysimeters within each classification group, with sample size
593 (n) specified in the legend. Shaded areas represent ± 1 standard deviation. Thin grey lines show individual MB
594 trajectories of the remaining lysimeters in each group. Highlighted blue lines depict selected replicates
595 originating from and/or tested at distinct sites: (a) BL → BL (soil material from Bad Lauchstädt tested at its
596 origin), (b) DD → BL (soil material from Dedelow tested at Bad Lauchstädt), and (c) BL → SE (soil material
597 from Bad Lauchstädt tested at Selhausen). These examples illustrate contrasting temporal patterns in hydraulic
598 response, ranging from sustained stability to progressive divergence from the trained site dynamics.

599 **Table 1:** Resilience of soil water content response function for the four soil materials translocated to Bad
600 Lauchstädt and Selhausen. The ‘type’ describes the class of response function of the individual lysimeters (S for
601 ‘stable’, R for ‘resilient’ and C for ‘changed’). The ‘drift’ is the average value $|\text{MB}_{2023} - \text{MB}_{2015}|$ of the three
602 lysimeters with the difference in Mean Bias (MB) between years 2023 and 2015. The ‘amplitude’ is the maximum

603 difference of the Mean Bias between the first year (2015) and the years between 2018 and 2022 (denoted as year
 604 20xx).

	Located at Bad Lauchstädt			Located at Selhausen		
	Type	Drift	Amplitude	Type	Drift	Amplitude
Dedelow	S, R, C	1.09	1.76	R, C, C	1.72	2.11
Bad Lauchstädt	S, S, R	0.94	1.36	R, C, C	2.15	2.99
Sauerbach	C, C, C	2.17	3.73	C, C, C	3.38	4.24
Selhausen	S, R, C	0.96	2.24	S, S, R	0.47	1.78

605

606 4. Discussion

607 The results presented in Section 3 demonstrate that the model can reproduce soil water content dynamics
 608 reliably under stable conditions (as indicated by high NSE values), but it exhibits limitations when soils
 609 undergo persistent changes in hydraulic behaviour or are exposed to a different climate. Several soils
 610 showed a shift in the wet range, indicating that differences in soil water content response cannot be
 611 explained by texture alone but reflect the combined effects of climatic conditions and structural
 612 evolution. Based on these findings, the following discussion evaluates how assumptions of static
 613 hydraulic behaviour and the response function affect model performance, examines the role of NSE and
 614 MB in identifying evolving system dynamics, and reflects on the broader implications for long-term
 615 modelling and soil water content monitoring.

616 4.1 Soil–Climate Interactions as Drivers of Hydraulic Response Function

617 The predictive success of data-driven models depends not only on the physical properties of soils but
 618 also on the climatic context in which those properties developed and continue to function. The present
 619 study shows that soils exhibit the most consistent replicate behaviour when evaluated under climate
 620 conditions similar to those of their origin, where gradual climatic changes over time have allowed their
 621 structure to adjust naturally. When exposed to faster or contrasting climatic shifts, as in translocated
 622 settings, the soil response becomes less predictable and less stable. This is demonstrated in Table S1 in
 623 the Supplementary Material, which lists the average trends (difference in MB between 2023 and 2015)
 624 and amplitudes (difference in MB between 2015 and the dry years) for three lysimeter replicates. Only
 625 for the three lysimeters at the original locations (Bad Lauchstädt or Selhausen) were both drift and

626 amplitude below the stability threshold of 1.52% and could be classified as ‘stable’ as a group of
627 lysimeters.

628 This suggests that the function of the soil system cannot be meaningfully decoupled from its climatic
629 history. Soils may develop pore arrangements, aggregation patterns and, as a consequence, soil water
630 retention characteristics that reflect long-term adaptation to local hydrological regimes. When these
631 soils are translocated to environments with contrasting precipitation and atmospheric demand, their
632 hydraulic response can shift in ways that are not captured by static texture-based estimates of soil
633 hydraulic properties. Alternative pore-scale processes, including slowly reversible swell–shrink
634 behaviour and non-equilibrium preferential flow, may also contribute to the observed shifts in apparent
635 SWRC behaviour. Recent large-scale analyses have demonstrated statistically significant impacts of
636 climatic factors on soil pore space organisation and laboratory-measured retention characteristics
637 (Hirmas et al., 2018; Klöffel et al., 2024), providing independent support for the plausibility of climate-
638 driven modification of soil hydraulic response.

639 Such context-dependent behaviour highlights the limitation of the common assumption that soils with
640 the same texture will show comparable retention across regions, an assumption often made in the
641 absence of better descriptors. While laboratory-measured SWRCs show strong and well-established
642 correlations with texture across climatic gradients, particularly in the dry range, experimental evidence
643 collected under natural field conditions indicates that this simplified description does not always hold
644 (Hannes et al., 2016; Robinson et al., 2016; Aqel et al., 2024). In our case, even soils with similar
645 textural composition exhibited different levels of model agreement depending on climate, highlighting
646 that physical similarity (e.g., soil texture) does not guarantee functional equivalence in retention. For
647 example, Selhausen-origin soils achieved higher NSE values when translocated to Bad Lauchstädt,
648 likely because the model was trained under similar dry climatic conditions. However, classification
649 results showed that these soils retained greater stability at their origin, suggesting that predictive success
650 under familiar climatic forcing does not necessarily imply hydraulic consistency. After the 2018
651 drought, the Selhausen soils translocated to Bad Lauchstädt converged towards similar dynamics across
652 replicates, with MB stabilizing close to zero, indicating that their response functions adjusted
653 consistently to the drier climate (see Fig. S2 in the Supplementary Material). However, a clear carry-

654 over effect was observed: soil water in the upper 10 cm was not fully replenished during the wet phase
655 of autumn and winter 2019 and only reached comparable, though slightly lower, values in winter 2020.
656 A comparable multi-year legacy across the full soil column was reported in the TERENO-SOILCan
657 lysimeter network by Groh et al. (2020).

658 All mentioned points underscore the importance of including a very broad range of climatic forcing in
659 the assessment of soil model transferability, as demonstrated by Groh et al. (2022). Our results also
660 suggest that future efforts to generalise hydrological models should consider training under a range of
661 climatic conditions to capture the full expression of soil–climate interactions, rather than relying on a
662 single static representation. From a process-based perspective, these findings reflect that climate does
663 not simply modulate soil water content inputs but actively shapes the retention and release behaviour
664 of the soil pore network by driving changes in soil hydraulic response. While management practices
665 across sites were similar, minor differences in tillage and fertilization cannot be completely excluded
666 and may have influenced soil structure and water retention. In addition, monitoring of soil organic
667 matter over time would be useful to link changes in the response function and structure-related soil
668 hydraulic properties to biological processes. Another mechanism that could result in structural changes
669 is swelling and shrinking of the soils with considerable clay content (three soils with ~20% clay).
670 Nonetheless, the dominant control remains climatic forcing, which makes this consideration particularly
671 relevant for climate-change experiments: models calibrated under past climatic conditions may not
672 remain valid under the rapid climatic shifts projected for the coming decades. Neglecting this evolving
673 soil–climate feedback could lead to substantial underestimation of future changes in soil hydraulic
674 behaviour and associated ecosystem responses.

675 4.2 High Predictive Performance Can Mask System Evolution

676 Although several lysimeters achieved high predictive performance as expressed by high NSE values
677 (Fig. 9), systematic trends in MB suggest that the underlying retention behaviour and soil water content
678 response function may have shifted (Fig. 10 and Table 1). This was most apparent in Dedelow soils
679 translocated to Bad Lauchstädt, where the model maintained high NSE values, but the MB increased
680 across years (see Fig. S3). The corresponding shifts in the soil water retention curves confirmed a

681 gradual change in how the soil retained water, despite the model continuing to predict moisture levels
682 accurately.

683 This suggests that local changes in hydraulic behaviour can occur without immediate deterioration in
684 model fit. The predictive framework remained effective in capturing the general moisture dynamics,
685 but the relationship between matric potential and water content was no longer consistent with that
686 observed during training. These findings highlight that high model accuracy does not guarantee stability
687 in soil hydraulic behaviour, particularly under changing environmental conditions. Identifying such
688 divergence early is critical for maintaining reliable predictions in long-term monitoring.

689 4.3 Implications for Monitoring, Remote Sensing, and Soil Health

690 The classification outcomes across all lysimeters highlight the role of site memory and hydraulic
691 resilience in maintaining soil water response under climatic stress. Soils assessed at their origin were
692 more frequently classified as ‘stable’ or ‘resilient’ (e.g., Selhausen at Selhausen), while those
693 translocated to different locations were more likely to be classified as ‘changed’ (e.g., Sauerbach at Bad
694 Lauchstädt). As stated in the Materials and Methods section, this classification as ‘changed’ is affected
695 by the length of the observation window and does not allow for a definitive decision between a persistent
696 change to a new response function and a manifestation of a slow recovery rate. Regardless of future
697 developments, these patterns indicate that soil hydraulic behaviour shaped by long-term climatic
698 adaptation may change when soils are exposed to new environmental conditions. The presented
699 methods allow the detection of emerging shifts in soil hydraulic behaviour that may be relevant for soil
700 health assessment and could serve as indicators of deteriorating soil health status.

701 This has direct implications for long-term monitoring and remote sensing. Our model framework, which
702 avoids reliance on matric potential data and instead uses moisture state categories and decomposed
703 climatic features, is compatible with satellite-derived products. As remote sensing missions increasingly
704 provide continuous global soil water content estimates, the proposed framework could be adapted for
705 large-scale assessment of soil system stability. Furthermore, under scenarios of future climate change,
706 where shifts in precipitation patterns and evaporative demand are expected, data-driven models trained

707 on historical data may become progressively outdated. The presented residual-based approach
708 (quantifying MB) enables early detection of such divergence, offering a method for identifying when
709 model retraining or reparameterisation is needed to maintain predictive reliability under non-stationary
710 conditions.

711 5. Summary and Conclusions

712 Temporal variations in topsoil water content control near-surface hydraulic conditions, infiltration,
713 evaporation, and gas exchange, thereby shaping soil water dynamics and physical soil functioning.
714 Reliable information about soil water content dynamics in response to atmospheric conditions is thus
715 essential for detecting and mitigating critical changes in soil hydraulic behaviour. This response
716 depends on soil hydraulic properties that are traditionally characterised by a time-invariant and
717 unambiguous relationship between matric potential, water content, and hydraulic conductivity as
718 deduced from small-scale lab experiments. In this study, we developed and applied a feed-forward
719 neural network combined with seasonal trend analysis of climatic time series to quantify the soil water
720 content response function after an extreme drought in the summer of 2018 in Germany. By analysing
721 the time series of topsoil water content measured at two lysimeter stations of the TERENO-SOILCan
722 network, we summarize the conclusions on the soil water content response function as follows:

- 723 • 50% of the lysimeters showed changes in soil water content dynamics after the dry summer of
724 2018 without recovery until 2023.
- 725 • The remaining lysimeters showed resilient behaviour, and the soil water content response
726 function was not permanently changed.
- 727 • Changes in the soil water content response function were manifested as (i) temporal trends in
728 prediction error (mean bias) and (ii) shifts in the soil water retention function.
- 729 • The soil water content response function is adapted to climatic conditions as manifested by (i)
730 minimal changes in the lysimeters that were not translocated and (ii) reduced model
731 performance for applications of a response function that was determined for another climate.

732 • Good model performance as expressed by high Nash-Sutcliffe efficiency values does not
733 correspond to a stable soil water content response function that was only detected by temporal
734 trends in error metrics.

735 The study revealed that intense drought events can induce lasting changes in soil hydraulic properties,
736 but the degree of resilience depends on both soil type and climatic conditions. We argue that soils which
737 developed under a broader range of climatic conditions may possess soil hydraulic properties that
738 enhance resilience to subsequent drought, and that this inherited behaviour persists after translocation
739 to a new climatic regime. Because the presented model framework does (i) not aim to accurately predict
740 soil water content time series and (ii) only requires categorical water content information ('stable',
741 'resilient', 'changed'), it can be applied at larger scales using remote sensing data that do not provide
742 accurate soil water content values but reliable trends, enabling the detection of changes in hydraulic
743 behaviour at the ecosystem scale.

744 Code availability

745 The codes developed for this study are available from the authors upon reasonable request.

746 Data availability

747 The TERENO-SOILCan lysimeter data used in this study are not publicly available. Access to the data
748 is restricted and subject to approval by the TERENO-SOILCan data provider and the TERENO data
749 management team. The data may be obtained from the corresponding author upon reasonable request
750 and with the appropriate permissions.

751 Author contributions

752 NA, AC, and PL designed the study. NA and PL conducted the research. NA developed the model and
753 wrote the code. NA and PL prepared the manuscript with contributions of all co-authors. JG and RG
754 provided and quality-controlled the lysimeter data.

755 Competing interests

756 The authors declare that they have no conflict of interest.

757 Financial support

758 This research is part of the project AI4SoilHealth of the European Union’s Horizon research and
759 innovation program (grant agreement No. 101086179). This work has received funding from the Swiss
760 State Secretariat for Education, Research and Innovation (SERI).

761 Acknowledgements

762 We acknowledge the support of TERENO and SOILCan, which were funded by the Helmholtz
763 Association (HGF) and the Federal Ministry of Education and Research (BMBF, Germany).

764 We would like to thank Ines Merbach, Sylvia Schmögner, Werner Küpper, Philipp Meulendick,
765 Ferdinand Engels, Antonio Voss, Leander Fürst and Rainer Harms for their kind support at the lysimeter
766 stations in Bad Lauchstädt and Selhausen. We thank Hans-Jörg Vogel for his constructive feedback and
767 insightful comments on the manuscript.

768 References

769 Allen, R. G., Pereira, L. S., Raes, D., and Smith, M.: Crop evapotranspiration – Guidelines for
770 computing crop water requirements, FAO Irrigation and Drainage Paper 56, Food and
771 Agriculture Organization of the United Nations, Rome, 300 pp., 2006.

772 Aqel, N., Reusser, L., Margreth, S., Carminati, A., and Lehmann, P.: Prediction of hysteretic
773 matric potential dynamics using artificial intelligence: application of autoencoder neural
774 networks, *Geosci. Model Dev.*, 17, 6949–6966, <https://doi.org/10.5194/gmd-17-6949-2024>,
775 2024.

776 Blöschl, G., Bierkens, M. F. P., Chambel, A., Cudennec, C., Destouni, G., Fiori, A., Kirchner, J. W.,
777 McDonnell, J. J., Savenije, H. H. G., Sivapalan, M., Stumpp, C., Toth, E., Volpi, E., Carr, G.,
778 Lupton, C., Salinas, J., Széles, B., Viglione, A., Aksoy, H., and Zhang, Y.: Twenty-three unsolved
779 problems in hydrology (UPH) – a community perspective, *Hydrol. Sci. J.*, 64, 1141–1158,
780 <https://doi.org/10.1080/02626667.2019.1620507>, 2019.

781 Boergens, E., Güntner, A., Sips, M., Schwatke, C., and Dobsław, H.: Interannual variations of
782 terrestrial water storage in the East African Rift region, *Hydrol. Earth Syst. Sci.*, 28, 4733–4754,
783 <https://doi.org/10.5194/hess-28-4733-2024>, 2024.

784 Bogena, H. R., Huisman, J. A., Güntner, A., Hübner, C., Kusche, J., Jonard, F., Vey, S., and
785 Vereecken, H.: Emerging methods for noninvasive sensing of soil moisture dynamics from field
786 to catchment scale: a review, *WIREs Water*, 2, 635–647, <https://doi.org/10.1002/wat2.1097>,
787 2015.

788 Brocca, L., Melone, F., Moramarco, T., Wagner, W., Naeimi, V., Bartalis, Z., and Hasenauer, S.:
789 Improving runoff prediction through the assimilation of the ASCAT soil moisture product,
790 *Hydrol. Earth Syst. Sci.*, 14, 1881–1893, <https://doi.org/10.5194/hess-14-1881-2010>, 2010.

791 Cleveland, R. B., Cleveland, W. S., McRae, J. E., and Terpenning, I.: STL: A seasonal-trend
792 decomposition procedure based on LOESS, *J. Off. Stat.*, 6, 3–73, 1990.

793 Detty, J. M. and McGuire, K. J.: Threshold changes in storm runoff generation at a till-mantled
794 headwater catchment, *Water Resour. Res.*, 46, W07525,
795 <https://doi.org/10.1029/2009WR008102>, 2010.

796 Deutscher Wetterdienst (DWD) Climate Data Center (CDC): Historical daily precipitation data,
797 station Leipzig/Halle (ID 2932), available at: <https://www.dwd.de/cdc>, last access: 28 August
798 2025, 2025.

799 Fatichi, S., Or, D., Walko, R., Vereecken, H., Young, M. H., Ghezzehei, T. A., Hengl, T., Kollet, S.,
800 Agam, N., and Avissar, R.: Soil structure is an important omission in Earth system models, *Nat.*
801 *Commun.*, 11, 522, <https://doi.org/10.1038/s41467-020-14411-z>, 2020.

802 Fu, Z., Hu, W., Beare, M., Thomas, S., Carrick, S., Dando, J., Langer, S., Müller, K., Baird, D., and
803 Lilburne, L.: Land use effects on soil hydraulic properties and the contribution of soil organic
804 carbon, *J. Hydrol.*, 602, 126741, <https://doi.org/10.1016/j.jhydrol.2021.126741>, 2021.

805 Groh, J., Diamantopoulos, E., Duan, X., Ewert, F., Heinlein, F., Herbst, M., Holbak, M., Kamali, B.,
806 Kersebaum, K.-C., Kuhnert, M., Nendel, C., Priesack, E., Steidl, J., Sommer, M., Pütz, T.,
807 Vanderborght, J., Vereecken, H., Wallor, E., Weber, T. K. D., and Gerke, H. H.: Same soil,
808 different climate: crop model intercomparison on translocated lysimeters, *Vadose Zone J.*, 21,
809 e20202, <https://doi.org/10.1002/vzj2.20202>, 2022.

810 Groh, J., Vanderborght, J., Pütz, T., Vogel, H.-J., Gründling, R., Rupp, H., Rahmati, M., Sommer,
811 M., Vereecken, H., and Gerke, H. H.: Responses of soil water storage and crop water use
812 efficiency to changing climatic conditions: a lysimeter-based space-for-time approach, *Hydrol.*
813 *Earth Syst. Sci.*, 24, 1211–1225, <https://doi.org/10.5194/hess-24-1211-2020>, 2020.

814 Hannes, M., Wollschläger, U., Wöhling, T., and Vogel, H.-J.: Revisiting hydraulic hysteresis based
815 on long-term monitoring of hydraulic states in lysimeters, *Water Resour. Res.*, 52, 3847–3865,
816 <https://doi.org/10.1002/2015WR018319>, 2016.

817 Hari, V., Rakovec, O., Markonis, Y., Hanel, M., and Kumar, R.: Increased future occurrences of
818 the exceptional 2018–2019 Central European drought under global warming, *Sci. Rep.*, 10,
819 12207, <https://doi.org/10.1038/s41598-020-68872-9>, 2020.

820 Herbrich, M. and Gerke, H. H.: Scales of water retention dynamics observed in eroded Luvisols
821 from an arable postglacial soil landscape, *Vadose Zone J.*, 16, 1–12,
822 <https://doi.org/10.2136/vzj2017.01.0003>, 2017.

823 Hirmas, D. R., Giménez, D., Nemes, A., Kerry, R., Brunzell, N. A., and Wilson, C. J.: Climate-
824 induced changes in continental-scale soil macroporosity may intensify water cycle, *Nature*, 561,
825 100–103, <https://doi.org/10.1038/s41586-018-0463-x>, 2018.

826 Holling, C. S.: Resilience and stability of ecological systems, IIASA Research Report RR-73-003
827 (Reprint), IIASA, Laxenburg, Austria, reprinted from *Annual Review of Ecology and Systematics*,
828 4, 1–23, <https://pure.iiasa.ac.at/id/eprint/26/1/RP-73-003.pdf>, 1973.

829 Hrachowitz, M., Savenije, H. H. G., Blöschl, G., McDonnell, J. J., Sivapalan, M., Pomeroy, J. W.,
830 Arheimer, B., Blume, T., Clark, M. P., Ehret, U., Fenicia, F., Freer, J. E., Gelfan, A., Gupta, H. V.,
831 Hughes, D. A., Hut, R. W., Montanari, A., Pande, S., Tetzlaff, D., and Cudennec, C.: A decade of
832 Predictions in Ungauged Basins (PUB) – a review, *Hydrol. Sci. J.*, 58, 1198–1255,
833 <https://doi.org/10.1080/02626667.2013.803183>, 2013.

834 Jarvis, N. J., Coucheney, E., Lewan, E., Klöffel, T., Meurer, K. H. E., Keller, T., and Larsbo, M.:
835 Interactions between soil structure dynamics, hydrological processes and organic matter
836 cycling: a new soil-crop model, *Eur. J. Soil Sci.*, 75, e13455, <https://doi.org/10.1111/ejss.13455>,
837 2024.

838 Kingma, D. P. and Ba, J.: Adam: A method for stochastic optimization, *Proceedings of the*
839 *International Conference on Learning Representations (ICLR)*, 2015,
840 <https://arxiv.org/abs/1412.6980>, 2015.

841 Klöffel, T., Barron, J., Nemes, A., Giménez, D., and Jarvis, N. J.: Soil, climate, time and site
842 factors as drivers of soil structure evolution in agricultural soils from a temperate-boreal
843 region, *Geoderma*, 442, 116772, <https://doi.org/10.1016/j.geoderma.2024.116772>, 2024.

844 Kratzert, F., Klotz, D., Shalev, G., Klambauer, G., Hochreiter, S., and Nearing, G. S.: Towards
845 learning universal, regional, and local hydrological behaviours via machine learning applied to
846 large-sample datasets, *Hydrol. Earth Syst. Sci.*, 23, 5089–5110, <https://doi.org/10.5194/hess-23-5089-2019>, 2019.

848 Kuzyakov, Y. and Zamanian, K.: Reviews and syntheses: Agropedogenesis – humankind as the
849 sixth soil-forming factor and attractors of agricultural soil degradation, *Biogeosciences*, 16,
850 4783–4803, <https://doi.org/10.5194/bg-16-4783-2019>, 2019.

851 Lehmann, P., Bickel, S., Wei, Z., and Or, D.: Physical constraints for improved soil hydraulic
852 parameter estimation by pedotransfer functions, *Water Resour. Res.*, 56, e2019WR025963,
853 <https://doi.org/10.1029/2019WR025963>, 2020.

854 Liu, J., Hughes, D., Rahmani, F., Lawson, K., and Shen, C.: Evaluating a global soil moisture
855 dataset from a multitask model (GSM3 v1.0) with potential applications for crop threats,
856 *Geosci. Model Dev.*, 16, 1553–1567, <https://doi.org/10.5194/gmd-16-1553-2023>, 2023.

857 Liu, J., Rahmani, F., Lawson, K., and Shen, C.: A multiscale deep learning model for soil moisture
858 integrating satellite and in situ data, *Geophys. Res. Lett.*, 49, e2021GL096847,
859 <https://doi.org/10.1029/2021GL096847>, 2022.

860 Liu, Y. Y., Parinussa, R. M., Dorigo, W. A., De Jeu, R. A. M., Wagner, W., van Dijk, A. I. J. M.,
861 McCabe, M. F., and Evans, J. P.: Developing an improved soil moisture dataset by blending
862 passive and active microwave satellite-based retrievals, *Hydrol. Earth Syst. Sci.*, 15, 425–436,
863 <https://doi.org/10.5194/hess-15-425-2011>, 2011.

864 Lu, L., Shin, Y., Su, Y., and Karniadakis, G. E.: Dying ReLU and initialization: theory and numerical
865 examples, *Commun. Comput. Phys.*, 28, 1671–1706, [https://doi.org/10.4208/cicp.OA-2020-](https://doi.org/10.4208/cicp.OA-2020-0165)
866 0165, 2020.

867 Melsen, L. A. and Guse, B.: Climate change impacts model parameter sensitivity – implications
868 for calibration strategy and model diagnostic evaluation, *Hydrol. Earth Syst. Sci.*, 25, 1307–
869 1332, <https://doi.org/10.5194/hess-25-1307-2021>, 2021.

870 Milly, P. C. D., Betancourt, J., Falkenmark, M., Hirsch, R. M., Kundzewicz, Z. W., Lettenmaier, D.
871 P., and Stouffer, R. J.: Stationarity is dead: Whither water management?, *Science*, 319, 573–
872 574, <https://doi.org/10.1126/science.1151915>, 2008.

873 Montanari, A., Young, G., Savenije, H. H. G., Hughes, D., Wagener, T., Ren, L.-L., Koutsoyiannis,
874 D., Cudennec, C., Toth, E., Grimaldi, S., Blöschl, G., Sivapalan, M., Beven, K., Gupta, H., Hipsey,
875 B., Schaefli, B., Arheimer, B., Boegh, E., Schymanski, S. J., and Belyaev, V.: “Panta Rhei—
876 Everything Flows”: change in hydrology and society—The IAHS Scientific Decade 2013–2022,
877 *Hydrol. Sci. J.*, 58, 1256–1275, <https://doi.org/10.1080/02626667.2013.809088>, 2013.

878 Montesinos López, O. A., Montesinos López, A., and Crossa, J.: Fundamentals of artificial neural
879 networks and deep learning, in: *Multivariate Statistical Machine Learning Methods for*
880 *Genomic Prediction*, Springer International Publishing, Cham, 379–425,
881 https://doi.org/10.1007/978-3-030-89010-0_10, 2022.

882 Moriasi, D. N., Arnold, J. G., Van Liew, M. W., Bingner, R. L., Harmel, R. D., and Veith, T. L.:
883 Model evaluation guidelines for systematic quantification of accuracy in watershed
884 simulations, *Trans. ASABE*, 50, 885–900, <https://doi.org/10.13031/2013.23153>, 2007.

885 Moriasi, D. N., Gitau, M. W., Pai, N., and Daggupati, P.: Hydrologic and water quality models:
886 Performance measures and evaluation criteria, *Trans. ASABE*, 58, 1763–1785,
887 <https://web.ics.purdue.edu/~mgitau/pdf/Moriasi%20et%20al%202015.pdf>, 2015.

888 Mosavi, A., Ozturk, P., and Chau, K.-W.: Flood prediction using machine learning models:
889 literature review, *Water*, 10, 1536, <https://doi.org/10.3390/w10111536>, 2018.

890 Nash, J. E. and Sutcliffe, J. V.: River flow forecasting through conceptual models part I — A
891 discussion of principles, *J. Hydrol.*, 10, 282–290, [https://doi.org/10.1016/0022-1694\(70\)90255-](https://doi.org/10.1016/0022-1694(70)90255-6)
892 6, 1970.

893 Nearing, G. S., Kratzert, F., Sampson, A. K., Pelissier, C. S., Klotz, D., Frame, J. M., Prieto, C., and
894 Gupta, H. V.: What role does hydrological science play in the age of machine learning?, *Water*
895 *Resour. Res.*, 57, e2020WR028091, <https://doi.org/10.1029/2020WR028091>, 2021.

896 O, S. and Orth, R.: Global soil moisture data derived through machine learning trained with in-
897 situ measurements, *Sci. Data*, 8, 170, <https://doi.org/10.1038/s41597-021-00964-1>, 2021.

898 Pütz, T., Kiese, R., Wollschläger, U., Groh, J., Rupp, H., Zacharias, S., Priesack, E., Gerke, H. H.,
899 Gasche, R., Bens, O., Borg, E., Baessler, C., Kaiser, K., Herbrich, M., Munch, J.-C., Sommer, M.,
900 Vogel, H.-J., Vanderborght, J., and Vereecken, H.: TERENO-SOILCan: a lysimeter-network in
901 Germany observing soil processes and plant diversity influenced by climate change, *Environ.*
902 *Earth Sci.*, 75, 1242, <https://doi.org/10.1007/s12665-016-6031-5>, 2016.

903 Quintana, J. R., Martín-Sanz, J. P., Valverde-Asenjo, I., and Molina, J. A.: Drought differently
904 destabilizes soil structure in a chronosequence of abandoned agricultural lands, *Catena*, 222,
905 106871, <https://doi.org/10.1016/j.catena.2022.106871>, 2023.

906 Reichstein, M., Camps-Valls, G., Stevens, B., Jung, M., Denzler, J., Carvalhais, N., and Prabhat:
907 Deep learning and process understanding for data-driven Earth system science, *Nature*, 566,
908 195–204, <https://doi.org/10.1038/s41586-019-0912-1>, 2019.

909 Robinson, D. A., Jones, S. B., Lebron, I., Reinsch, S., Domínguez, M. T., Smith, A. R., Jones, D. L.,
910 Marshall, M. R., and Emmett, B. A.: Experimental evidence for drought induced alternative
911 stable states of soil moisture, *Sci. Rep.*, 6, 20018, <https://doi.org/10.1038/srep20018>, 2016.

912 Robinson, D. A., Hopmans, J. W., Filipović, V., van der Ploeg, M., Lebron, I., Jones, S. B., Reinsch,
913 S., Jarvis, N., and Tuller, M.: Global environmental changes impact soil hydraulic functions
914 through biophysical feedbacks, *Glob. Change Biol.*, 25, 1895–1904,
915 <https://doi.org/10.1111/gcb.14626>, 2019.

916 Robinson, D. A., Nemes, A., Reinsch, S., Radbourne, A., Bentley, L., and Keith, A. M.: Global
917 meta-analysis of soil hydraulic properties on the same soils with differing land use, *Sci. Total
918 Environ.*, 852, 158506, <https://doi.org/10.1016/j.scitotenv.2022.158506>, 2022.

919 Sainju, U. M., Liptzin, D., and Jabro, J. D.: Relating soil physical properties to other soil
920 properties and crop yields, *Sci. Rep.*, 12, 22025, <https://doi.org/10.1038/s41598-022-26619-8>,
921 2022.

922 Seneviratne, S. I., Corti, T., Davin, E. L., Hirschi, M., Jaeger, E. B., Lehner, I., Orlowsky, B., and
923 Teuling, A. J.: Investigating soil moisture–climate interactions in a changing climate: a review,
924 *Earth-Sci. Rev.*, 99, 125–161, <https://doi.org/10.1016/j.earscirev.2010.02.004>, 2010.

925 Shen, C., Laloy, E., Elshorbagy, A., Albert, A., Bales, J., Chang, F.-J., Ganguly, S., Hsu, K.-L., Kifer,
926 D., Fang, Z., Fang, K., Li, D., Li, X., and Tsai, W.-P.: HESS Opinions: Incubating deep-learning-
927 powered hydrologic science advances as a community, *Hydrol. Earth Syst. Sci.*, 22, 5639–5656,
928 <https://doi.org/10.5194/hess-22-5639-2018>, 2018.

929 Sun, W., Zhou, S., Yu, B., Zhang, Y., Keenan, T., and Fu, B.: Soil moisture–atmosphere
930 interactions drive terrestrial carbon–water trade-offs, *Commun. Earth Environ.*, 6, 169,
931 <https://doi.org/10.1038/s43247-025-02145-z>, 2025.

932 Tromp-van Meerveld, H. J. and McDonnell, J. J.: Threshold relations in subsurface stormflow: 1.
933 A 147-storm analysis of the Panola hillslope, *Water Resour. Res.*, 42, W02410,
934 <https://doi.org/10.1029/2004WR003778>, 2006.

935 Uber, M., Vandervaere, J.-P., Zin, I., Braud, I., Heistermann, M., Legoût, C., Molinié, G., and
936 Nord, G.: How does initial soil moisture influence the hydrological response? A case study from
937 southern France, *Hydrol. Earth Syst. Sci.*, 22, 6127–6146, [https://doi.org/10.5194/hess-22-
938 6127-2018](https://doi.org/10.5194/hess-22-6127-2018), 2018.

939 Vaze, J., Post, D. A., Chiew, F. H. S., Perraud, J.-M., Viney, N. R., and Teng, J.: Climate non-
940 stationarity – validity of calibrated rainfall–runoff models for use in climate change studies, *J.
941 Hydrol.*, 394, 447–457, <https://doi.org/10.1016/j.jhydrol.2010.09.018>, 2010.

942 Vereecken, H., Amelung, W., Bauke, S. L., Bogaen, H., Brüggemann, N., Montzka, C.,
943 Vanderborght, J., Bechtold, M., Blöschl, G., Carminati, A., Javaux, M., Konings, A. G., Kusche, J.,

- 944 Neuweiler, I., Or, D., Steele-Dunne, S., Verhoef, A., Young, M., and Zhang, Y.: Soil hydrology in
945 the Earth system, *Nat. Rev. Earth Environ.*, 3, 573–587, [https://doi.org/10.1038/s43017-022-](https://doi.org/10.1038/s43017-022-00324-6)
946 00324-6, 2022.
- 947 Vereecken, H., Huisman, J. A., Bogaen, H., Vanderborght, J., Vrugt, J. A., and Hopmans, J. W.:
948 On the value of soil moisture measurements in vadose zone hydrology: a review, *Water*
949 *Resour. Res.*, 44, W00D06, <https://doi.org/10.1029/2008WR006829>, 2008.
- 950 Wankmüller, F. J. P., Delval, L., Lehmann, P., Baur, M. J., Cecere, A., Wolf, S., Or, D., Javaux, M.,
951 and Carminati, A.: Global influence of soil texture on ecosystem water limitation, *Nature*, 635,
952 631–638, <https://doi.org/10.1038/s41586-024-08089-2>, 2024.
- 953 Western, A. W. and Grayson, R. B.: The Tarrawarra data set: soil moisture patterns, soil
954 characteristics, and hydrological flux measurements, *Water Resour. Res.*, 34, 2765–2768,
955 <https://doi.org/10.1029/98WR01833>, 1998.
- 956 Xoplaki, E., Ellsäßer, F., Grieger, J., Nissen, K. M., Pinto, J. G., Augenstein, M., Chen, T.-C., and
957 Wolf, F.: Compound events in Germany in 2018: drivers and case studies, *Nat. Hazards Earth*
958 *Syst. Sci.*, 25, 541–564, <https://doi.org/10.5194/nhess-25-541-2025>, 2025.
- 959 Zehe, E. and Blöschl, G.: Predictability of hydrologic response at the plot and catchment scales:
960 role of initial conditions, *Water Resour. Res.*, 40, W10240,
961 <https://doi.org/10.1029/2003WR002869>, 2004.
- 962 Šimůnek, J., van Genuchten, M. T., and Šejna, M.: Recent developments and applications of the
963 HYDRUS computer software packages, *Vadose Zone J.*, 15, 1–25,
964 <https://doi.org/10.2136/vzj2016.04.0033>, 2016.